THE UNIVERSITY OF ALBERTA

RELEASE FORM

NAME OF AUTHOR Alastair George Beattie

TITLE OF THESIS A Photographic Study of the Kinematics of Natural Hailstones

DEGREE FOR WHICH THESIS WAS PRESENTED Master of Science

YEAR THIS DEGREE GRANTED 1975

THE UNIVERSITY OF ALBERTA

A PHOTOGRAPHIC STUDY OF THE KINEMATICS OF NATURAL HAILSTONES

by

©

ALASTAIR GEORGE BEATTIE

A THESIS

SUBMITTED TO THE FACULTY OF GRADUATE STUDIES AND RESEARCH

IN PARTIAL FULFILMENT OF THE REQUIREMENTS FOR THE DEGREE OF

MASTER OF SCIENCE

IN

METEOROLOGY

DEPARTMENT OF GEOGRAPHY

EDMONTON, ALBERTA

FALL, 1975

THE UNIVERSITY OF ALBERTA

FACULTY OF GRADUATE STUDIES AND RESEARCH

The undersigned certify that they have read, and recommend to the Faculty of Graduate Studies and Research, for acceptance, a thesis entitled "A Photographic Study of the Kinematics of Natural Hailstones," submitted by Alastair George Beattie in partial fulfilment of the requirements for the degree of Master of Science in Meteorology.

ABSTRACT

In attempting to study hailstone aerodynamics either experimentally or theoretically, several approximations are frequently made. Regular shapes, such as spheroids, may be assumed and models may be constrained to have fewer degrees of freedom than in free-fall. In order to avoid making any of these approximations in this study, hailshafts were sought out and natural hailstones were photographed under free-fall conditions near the ground.

This thesis describes the techniques used to photograph hail using a stereo camera pair and stroboscopic illumination. It describes the methods used to extract data from film and to determine accurate velocities from a pair of stereo photographs.

These methods are applied to two case studies, the principal one being a hailstorm which occurred on August 7, 1974 near to Ponoka, Alberta, the other being on August 18, 1974 near to Spruceview, Alberta. The results show that much of the hail fell faster than would be expected for spheroidal stones falling in a steady orientation with their minor axis vertical. This suggests that many of the stones were tumbling and that hailstone shape may be an important factor in determining fall velocities.

Finally recommendations are made for modifying the apparatus used so as to improve the quality and quantity of data which can be collected, with a view to observing in detail the rotation of tumbling hailstones.

ACKNOWLEDGEMENTS

I wish to express my gratitude to the people and organizations whose cooperation made this thesis possible.

Firstly I would like to thank my departmental supervisor, Dr. E. P. Lozowski, for his patient guidance throughout the course of this work, and also for organizing the field study. I also wish to thank Dr. R. B. Charlton and Dr. B. L. Clarke for serving on the examination committee.

My thanks go also to Mr. M. M. Oleskiw and Mr. T. M. Morrow who shared the work of operating the field experiment throughout the summer of 1974. I am also grateful for the helpful discussions held with several of my colleagues.

I wish to thank the Rotary Foundation of Rotary International for sponsoring my period of study at the University of Alberta by awarding me a Graduate Fellowship.

I would also like to thank the Alberta Department of Agriculture for supporting, through the Interim Weather Modification Board, this field study program.

TABLE OF CONTENTS

LIST OF TABLES

LIST OF FIGURES

LIST OF PLATES

Chapter 1. INTRODUCTION.

1.1 The General Problem.

Despite a wide variety of research in recent years, our knowledge of hail is far from complete. As noted by Mason (1971,p.332), hailstorms occur most frequently in the continental interiors of middle latitudes. The occurrence of hail, particularly of large stones, is usually associated with the occurrence of thunderstorms, but small hail may fall from clouds of lesser proportions (Mason, 1971,p.332).

The study of this phenomenon has been found to be very important owing to the severity of the damage caused in some areas by the large hailstorms which regularly occur there. Wojtiw and Summers (1972) estimated that in Alberta alone the annual drain on the economy through hail was, at that time, $30-40 million.

While many continental thunderstorms have hail associated with them, the hail generally reaches the ground in only a small area, compared to the area traversed by the storm. Consequently it was reported by Shands (1944), working in the State of Iowa, that, although a single station observed hail on only 1 in 12 thunderstorm days, the hail-thunderstorm ratio for the whole state was nearly one in two.

In badly afflicted areas much work has been done to try

to establish the overall pattern of hailstorm activity both with respect to time and place (see e.g. Douglas and Hitschfeld (1959), Held (1974)). There have also been several efforts to determine the surface coverage of hail associated with a particular thunderstorm in a known synoptic situation (e.g. Paul, 1973).

If significant relief is to be obtained from storm damage in the future, there must be advances in accurate forecasting and also in man's ability to control or modify storms. In order that there can be significant improvements in these fields, a greater understanding is required of both the macrophysics and the microphysics of these storms.

On the macroscale, storm development and progress have been traced in many instances using both photographic and radar techniques (Warner, 1973). These studies provide information concerning the overall structure of a storm and the development of the active cells within it. However, it is only recently that there has been the computational progress required to produce numerical models capable of simulating deep cumulonimbus convection (Miller and Pearce, 1974).

For a complete understanding of these storm systems an appreciation of the microphysics is essential. Much work remains to be done in order to determine with accuracy the processes involved in the growth and fall of most types of precipitation. In particular, in order that satisfactory

growth models can be developed, it is necessary to obtain an accurate account of the dynamics of hailstones, graupel, snowflakes and raindrops.

1.2 Aims of this Study.

Several workers have produced descriptions of the kinematics of a falling hailstone on the basis of theoretical studies of the aerodynamics of idealised bodies and measured aerodynamic parameters of such bodies (e.g. List et al, 1973). There have also been measurements made of the fallspeed, in the atmosphere, of hailstone models (Roos, 1972; Roos and Carte, 1973), but so far there have not been successful observations of natural hailstones in free-fall which could lead to any of the theoretical treatments being verified or refuted.

The purpose of this study is to attempt to provide the necessary information on hailstone kinematics by direct observation of natural hailstones in free-fall, using a stereo-photographic technique to record three-dimensional information about the hailstone trajectories. A similar technique has been used by Sasyo (1971) to study slow-falling snowflakes. Previous authors have concentrated their studies on large hail whereas, in this study, the discussion is of small hail. By international agreement (Atmospheric Environment Service of Canada, 1971, p.33) hail is precipitation consisting of 'balls' of ice each with a

maximum diameter greater than 5 mm; smaller solid precipitation of this type is called ice pellets or snow pellets. For the purposes of this study hail and ice or snow pellets are considered together as a single precipitation form and referred to as hail.

It was hoped that the kinematic information, thus obtained, would be sufficiently detailed to allow a useful comparison to be made with previous theoretical results.

1.3 Theoretical Studies of Hailstone Fall.

There have been a variety of approaches to the problem of hailstone aerodynamics. One of the earliest useful discussions on the subject is that of Bilham and Relf (1937), who produced calculations determining the terminal velocities of large hailstones by equating the drag of an ice sphere to its weight. The drag is customarily expressed in a form which relates it to the cross-sectional area of the body perpendicular to the flow ($\pi D^2/4$) and the dynamic pressure of the free stream flow ($\rho V^2/2$). Dividing the drag by the product of these quantities yields the non-dimensional parameter called the drag coefficient (C_D). Using the drag coefficient the drag and weight can be equated as follows:

$$\frac{1}{4}\pi D^2 C_D \rho_a V^2 = \frac{1}{6}\pi D^3 \rho_i g \qquad (1)$$

or

$$V^2 = \frac{2}{3} \frac{\rho_i}{\rho_a} \frac{g}{C_D} D \tag{2}$$

where D, ρ_i, V, C_D are respectively the diameter, density, terminal velocity and drag coefficient of the spherical hailstone, ρ_a is the air density and g is the acceleration due to gravity. It should be noted that modern convention, used by all subsequent authors, defines C_D to have twice the value of the C_D used in equation (1). Bilham and Relf deduced that in nature there should be an upper limit to the diameter of a hailstone (approx. 13 cm), at which the fallspeed increases greatly upon becoming supercritical and hence could no longer be balanced by a realistic updraft. That is the diameter which corresponds to the transition from laminar to turbulent airflow in the boundary layer about the hailstone (a Reynolds number of approximately 3×10^5 for smooth spheres).

An important advance in the theory of hailstone formation was soon made by Schumann (1938), who produced the first really quantitative treatment of hailstone growth. Ignoring the early stages of growth, he assumed a hailstone to grow as a spherical particle by sweeping up all the supercooled water droplets lying in its fallpath. He did realize that the growth rate of a hailstone would be limited by the rate at which it can dissipate the latent heat of fusion, and made allowance for this. Subsequently, more detailed calculations by Ludlam (1950), summarized by

Mason (1971,p.351), showed how fast freezing of moisture on the surface of a stone, alternating with periods when the liquid water collected by the stone is not completely frozen, due to ambient conditions of fallspeed, temperature and air liquid water content, can give rise to the onion-like clear-opaque layer structure commonly found in hailstones. Experimental verification of this work was provided by List (1959b) who carried out wind-tunnel investigations of the growth of hailstones in simulated atmospheric conditions.

After a considerable amount and variety of experimental work (described in section 1.4), undertaken by several workers, List et al (1973) produced a numerical simulation of a possible mode of fall of spheroidal hailstones. Wind-tunnel measurements of static drag, lift and torques were made for smooth oblate spheroids and the appropriate values were then inserted into the equations of motion, the resulting equations being solved numerically. The numerical simulation was initiated with a spheroid having a vertical minor axis and investigated the effect of a varying initial perturbation applied so as to cause oscillation which subsequently amplified to tumbling. This model was set up in accordance with previous observations by Knight and Knight (1970) that rotation about a horizontal major axis was a fundamental mode of motion, and it predicts in detail a possible fall pattern.

The numerical simulation approach was extended by Kry and List (1974) who considered the possibilities of spinning about a minor axis with simultaneous symmetrical gyration. They analysed the free-fall behaviour of oblate spheroids which are free to spin about the minor axis, with special attention to those motions thought to be significant for hailstones.

1.4 Previous Experimental Work.

In addition to the theoretical work discussed in section 1.3 there has been a large amount of experimental work which has contributed to our knowledge of the dynamics of hailstones and of other falling bodies.

Analysis of the bubble and crystal structure and the isotopic composition of a hailstone can give much information about the vertical component of the trajectory of a hailstone in a storm cell, during its growth (Macklin et al, 1970). Mossop (1971) studied the surface structure of irregular hailstones to try and derive an explanation for their shapes.

The analysis of hailstone structure, while providing corroborative evidence as to the accuracy of theories of hailstone aerodynamics, cannot prove these theories, so direct study of the fall of stones is necessary. Many authors have used hailstone models rather than actual hailstones for these studies (e.g. Roos, 1972; Roos and

Carte, 1973) and this makes instrumentation easier, as study of the methods used quickly shows. It also makes experiments much more repeatable than if actual hailstones are used. For some purposes 'idealised' models have been used, while for other experiments the models have been replicas, with respect to surface features, of large hailstones which have been collected previously. Methods for making such replica models are discussed by Carte (1971), the principal method being that of silicone rubber moulding.

With regard to the determination of the aerodynamics of hailstones, the first major advance on the work of Bilham and Relf did not come until List (1959a) published the results of his wind tunnel investigations, although separate relevant work had been under way on other falling bodies. Since, at that time, existing hail theories in mathematical form proceeded from the assumption that hailstones could be represented as smooth spheres, which they are in nature in a minority of cases, List carried out wind resistance tests in a wind-tunnel to determine, for various hailstones and models of graupel, the importance of deviations from Bilham and Relf's (1937) theoretical assumptions that hailstones may be approximated by spheres.

In a water tank, these hailstone models all fell at an orientation for which their speed of fall was a minimum. Comparing this fall-speed with that of ideal smooth spheres

having the same mass and density, differences of between 30% and 50% resulted. As these stones were smooth it was suggested that greater deviations could occur in nature. However the growth rate was little different from that previously obtained by Schumann (1938) because the product of fall-speed and cross-sectional area was approximately the same for spheres and for these hailstone models. This maintained growth rate coupled with slower fall-speed indicated that nature can produce larger and heavier hailstones than previous theoretical considerations had indicated.

For hailstones falling in the free atmosphere, these results were soon confirmed by Macklin and Ludlam (1961) who dropped large artificial hailstones containing metal foil from balloons and then followed the trajectory of each falling stone using a lock-follow radar. In this way they found that, owing to the different drag, their hailstones fell 15-20% more slowly than spheres of the same mass.

More recently Roos (1972), using theodolites, tracked replicas of a giant hailstone dropped from a helicopter. The original stone weighed 766 g and had large spikes confined mainly to one side. Roos was able to deduce its terminal velocity to be about 47 ms^{-1}. From this free-fall experiment and from wind-tunnel investigations, it was determined that, while oscillations occurred, the stone remained at an orientation such that the spiky face was

never downwards, i.e. the spikes always tended to trail.

Roos and Carte (1973) carried out a series of experiments, both in a vertical wind-tunnel and in free fall, to determine the aerodynamic properties and fall characteristics of replica models of ten non-spherical hailstones varying in mass from 1 g to 766 g. They developed an empirical formula to find the terminal velocity (V in ms^{-1}) from the mass (m in g) for the larger irregular stones, namely

$$V = 14.0\ m^{1/6} \qquad (3).$$

They also reported that a single protuberance, or several coplanar ones, tended to remain near to the horizontal plane during free fall. For several of these stones there was rotation about a vertical minor axis, and for those with a single horizontal spike there was rotation about the horizontal axis along the spike also. Oscillation about a horizontal axis was also common.

The tendency for a non-spherical stone to keep its major axis horizontal and for tumbling to occur on occasions was observed earlier by Knight and Knight (1970) while attempting to film a hailstone model in free-fall with the help of a sky-diver.

List and Schemenauer (1971) studied the fall characteristics of snowflake and graupel shaped models in a

water tank and observed that at low Reynolds numbers there tends to be steady motion but as Re increases, pitching sets in and finally the particle is subjected to continuous tumbling as it falls. This last observation, in particular, indicates that it might be beneficial to consider the progress in the study of other bodies with respect to their free-fall characteristics, in the hope that these studies may prove to be related to the problems facing us in the field of hailstone aerodynamics.

In the early 1950's work was done by Smith (1953) to determine the free-fall characteristics of an aircraft's jettisonable nose section. Observing that steady-state tumbling is a coplanar motion, he analysed tumbling and autorotation of the nose cone in question, considering most of the static and dynamic effects which could influence that body. He deliberately neglected wind fluctuations that may be important in many cases of hailstone tumbling for they may cause the initial perturbations to the body's steady fall which, he observes, may cause the onset of oscillation or tumbling. He comments that net moments, either driving or damping, can be induced by the motion of the body itself.

There have been two more recent studies which indicate some of the effects of wind perturbations. Wilmarth and Enlow (1969) and Fichtl (1971) carried out studies of the aerodynamic effects of fluctuations in the flow about spheres. These studies showed the sort of forces which

could be expected to act on small bodies as a result of airstream fluctuations. In the study of wind sensors, Fichtl neglected the effect of self-induced aerodynamic lift forces which may not be negligible for flatter bodies, including many hailstones.

Wilmarth, Hawk and Harvey (1964), studying the free-fall of discs, made some observations which are of particular interest in the light of List and Schemenauer's (1971) later observations. Slowly falling discs in a water tank were observed to have stable motion and a steady wake when they were in the low Reynolds number range (Re<100) corresponding to a steady wake behind a fixed disc in a fluid stream. In the Reynolds number range (100<Re<2000 approx.) where a stationary disc in an airflow sheds distinct vortices, a free-falling disc has a similar wake and oscillation of the disc sets in. At higher Reynolds numbers tumbling occurs. For a fuller description of the formation of these wakes, in the case of a fixed obstruction, see Goldstein (1938,p.556). In this case it was certain that the pressure fluctuation caused by vortex shedding was the driving force giving rise to the oscillations of the discs, and hence, in appropriate cases, tumbling.

Further studies of the fall patterns of idealised particles, in particular discs and oblate spheroids, were carried out by Stringham et al (1969). They describe in

detail the various fall patterns for their models and again stress the categorization according to Reynolds number regime, pointing out that the steadiness of a falling particle is dependent upon the directional stability of the resultant of the pressure forces in the wake, with the most non-spherical shapes and high Reynolds number causing the resultant force to be least stable.

A more recent study by Smith (1971) has sought to explain the auto-rotatory motion of a free wing. The rotation rate is related to the Strouhal number which is effectively a measure of wake stability (Goldstein, 1938).

This accumulation of observational evidence enabled the numerical modelling, mentioned in section 1.3, to be undertaken. It also provides predictions for the fall patterns of real hailstones, provided the models studied are good approximations to natural hailstones. So far there do not seem to have been any reports of observations of the fall patterns of natural hailstones in the atmosphere.

1.5 Fallspeed Formulae.

An important parameter determining the impact energy of hail (which is relevant to studies of hail damage), and also one of the easiest to determine from observation, is the terminal velocity. A variety of authors have determined, from theory or observation, formulae connecting terminal velocity to hailstone size which have not been previously

verified by studies of natural hail. It is therefore relevant to record some of these formulae, for comparison with the results obtained in this study.

Terminal velocity (V) is related to hailstone diameter (D) for a spherical hailstone by equating drag and weight as Bilham and Relf (1937) did. This gives, in modern notation,

$$V^2 = \frac{4}{3}\frac{\rho_i}{\rho_a}\frac{g}{C_D} D \qquad (2).$$

However the drag coefficient and hailstone density are not generally known while for non-spherical stones D is not always well-defined, so most authors have sought simpler empirical relationships. For use with any particular air density, the majority of authors in this field have favoured a formula of the form

$$V = c D^{1/2} \qquad (4)$$

where V is the terminal velocity in ms^{-1}, c is a constant, and D is some typical hailstone dimension in cm. By considering formulae in this form it is merely necessary to compare the values of the constant, c, obtained by different writers.

Wegener (1911), working from a simplified dynamic theory, was perhaps the first to suggest a relationship of the form given. He favoured a value of c of 8.8, for use at the surface, and of 14.45 for use at a height of 4 km. Bilham and Relf (1937) comment that a value of 14.1 would be

appropriate to the case of a spherical hailstone of pure ice at the surface.

List (1959a) presented a graphical illustration of how c varied according to particle shape, for hailstones and graupel. For his solutions, c lay within the approximate range 6.4 to 15. More recent workers have tended to favour the higher values of this range. Douglas (1964), when calculating hail-size distrubutions, chose the value 16.2 while Roos and Carte (1973) claimed 12.4 to be an average for large irregular hailstones, with 15 more appropriate for spherical bodies.

Strong (1974), studying hailfall at the surface in Central Alberta, the area used for the field study of this project, accepted C_D=0.60 as a mean drag coefficient for spherical hailstones falling in the area. The resulting velocity diameter relation, which he presents graphically, is very closely matched by

$$V = 13.59\ D^{1/2} \qquad (5)$$

It can be seen that while there is fair unanimity about the general form of the formula, there is little agreement about the value of c to be used to characterize natural hailstones.

Chapter 2. THE FIELD EXPERIMENT.

2.1 The Aims of the Field Work.

In order to investigate the motion of natural hailstones it is desirable to carry out one's observational program in the field, preferably in an area with a high incidence of hail. The study described here was carried out in Central Alberta, in cooperation with the Alberta Hail Project (ALHAP), by Dr. E. P. Lozowski and three graduate students, including the author.

The purpose of the work was to obtain stereographic photographs of hail in free-fall from which details of hailstone kinematics could be determined. The analysis of the films obtained was to become the work which is reported in this thesis.

The film records were obtained using a mobile photographic unit which could be located in a hailstorm. The design and operation of that unit will be discussed in this chapter.

2.2 Operation of the Experiment.

The Alberta Hail Project was originated in 1974 as the enlarged successor to Alberta Hail Studies which was formed in 1956 as a result of concern over heavy agricultural losses and enthusiastic meteorological research interest in

severe storms. ALHAP is concerned with the investigation of many aspects of Alberta hailstorms, and in particular the possible reduction of crop damage by seeding potential hail-bearing clouds with Silver Iodide. The project area is about 22,000 square miles in extent and lies between Edmonton and Calgary, centred on an operational base at Red Deer Industrial Airport, an air base about eleven kilometres southwest of Red Deer.

The mobile unit employed was a medium size van, normally with a crew of two to operate the equipment as well as to share the responsibilities of driver and navigator. In addition to the camera system, the van carried a hailcatcher for collecting timed sequential samples, a freezer, a 3kw A.C. generator, and radios for communication with the cloud seeding aircraft and the ALHAP radar control room. Radio communication allowed constant monitoring of storm cell locations and movements, thus greatly increasing the chances of positioning the van in the path of a significant storm cell.

The cameras were mounted close to the floor, approximately two feet from the side of the van, and were pointed to look out through a sliding side door while the vehicle was stopped (Plates 1,2). A backdrop consisting of two panels, each about 1.5 m high and 0.6 m wide, mounted at 138° to each other, was set up on the ground 0.8 m from the side of the van. The vehicle was pointed into the wind so

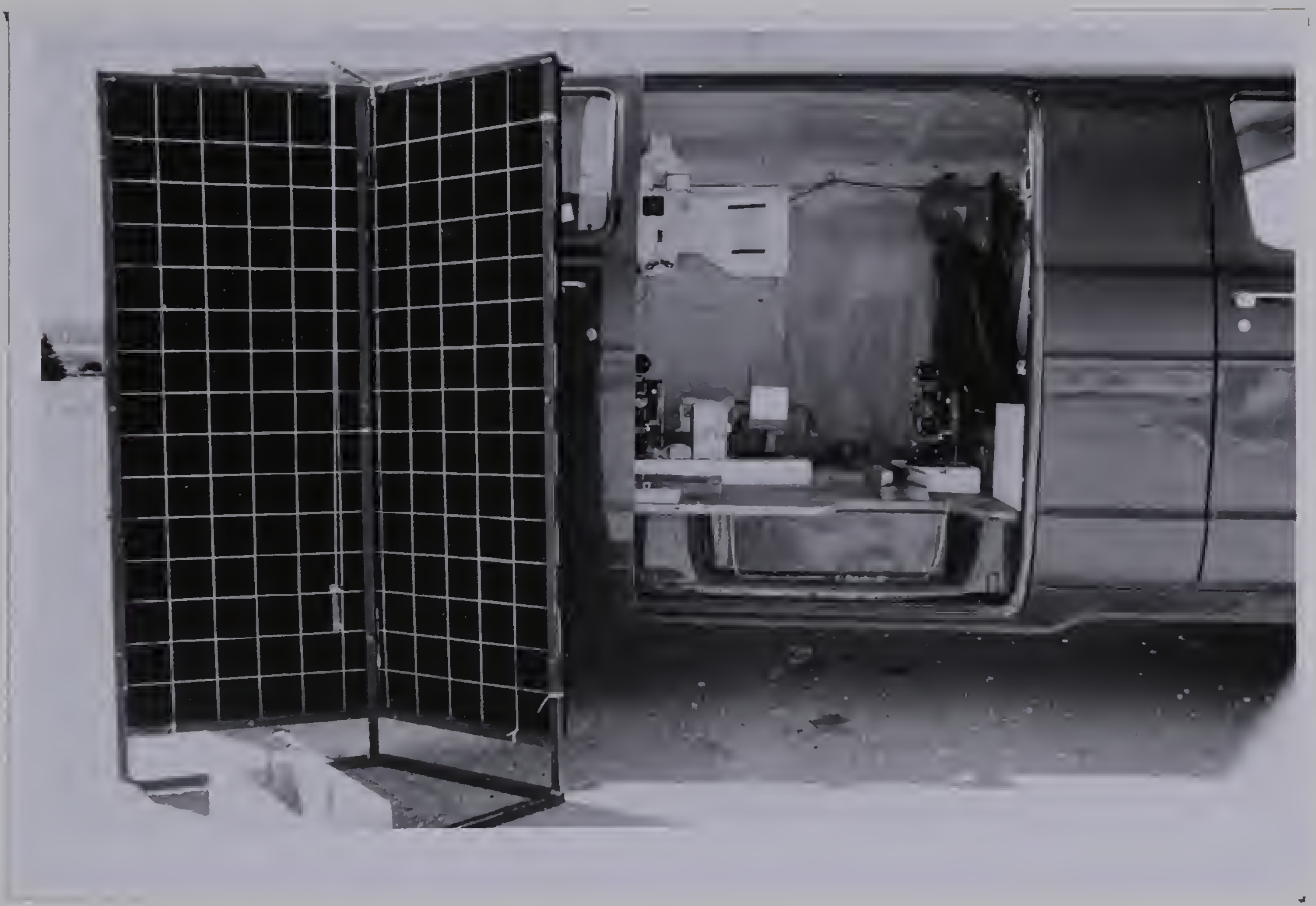

Plate 1. Horizontal view of camera arrangement, showing cameras and strobes, with backdrop displaced, and rotated by 180°.

Plate 2. Camera arrangement, as seen from above the backdrop which is in position.

that hailstones falling between the backdrop and the open door could be recorded on film, with a minimum number ricocheting off the van or the backdrop, and into the field of view of the cameras.

In order to provide protection from dust, mud and shock, which are significant on country roads, the cameras and lighting equipment were mounted in two foam rubber insulated boxes with removable upper sections and dust-tight seals. To avoid excessive optical distortion, the only protection afforded the cameras during the photography, other than that provided by the walls and roof of the van, was the provision of an ultraviolet filter over each lens. This arrangement afforded adequate protection against hail, provided that the van was pointed into the wind. Nevertheless, rain usually blew in through the open side door, and occasionally it drenched the cameras. The cameras were battery operated, but power for the lights was provided by the gasoline generator.

2.3 The Photographic Arrangement.

The photographic arrangement which was used initially consisted of a high-speed 16 mm cine camera with a half-mirrored backdrop. The details and operation of this setup are discussed by Lozowski et al (1975). One of the major difficulties of the system was that it produced a very small image size for hailstones on film, which made quantitative

analysis of the film difficult. In order to overcome this, and lesser practical difficulties, the system that was used for the present study consisted of two motor-driven 35mm SLR cameras, providing stereo photography without the use of a mirror, and using stroboscopic illumination.

The cameras used were Canon F-1's with 28 mm wide-angle lenses. These lenses have a diagonal viewing angle of 75° compared to the standard 50 mm lens's 46° (Suzuki, 1973). The cameras were mounted near the floor of the van, one metre apart, so as to be looking at the backdrop at an angle of 39.2° to each other. This arrangement is shown in Plates 1 and 2 and a plan view of the geometry is given in Figure 1. In this diagram, which shows how the equipment was set up under ideal conditions, A and B are the centres of the film frames of the two cameras and AO, BO are the optic axes of the cameras, where O is their point of intersection which lies on the spine of the backdrop and can be readily identified by a mark made on the spine. The backdrop consisted of two wooden panels faced with black velvet and with a 10cm square grid of white cord fixed in front of the velvet. Due to ground conditions, the backdrop was seldom perfectly positioned in practice; this is unimportant as the vertical was given by a plumb line suspended in front of the backdrop and the position of the optic axis on any photograph can be taken to be the intersection of the diagonals of that frame. The methods used to compensate for other departures from the designed

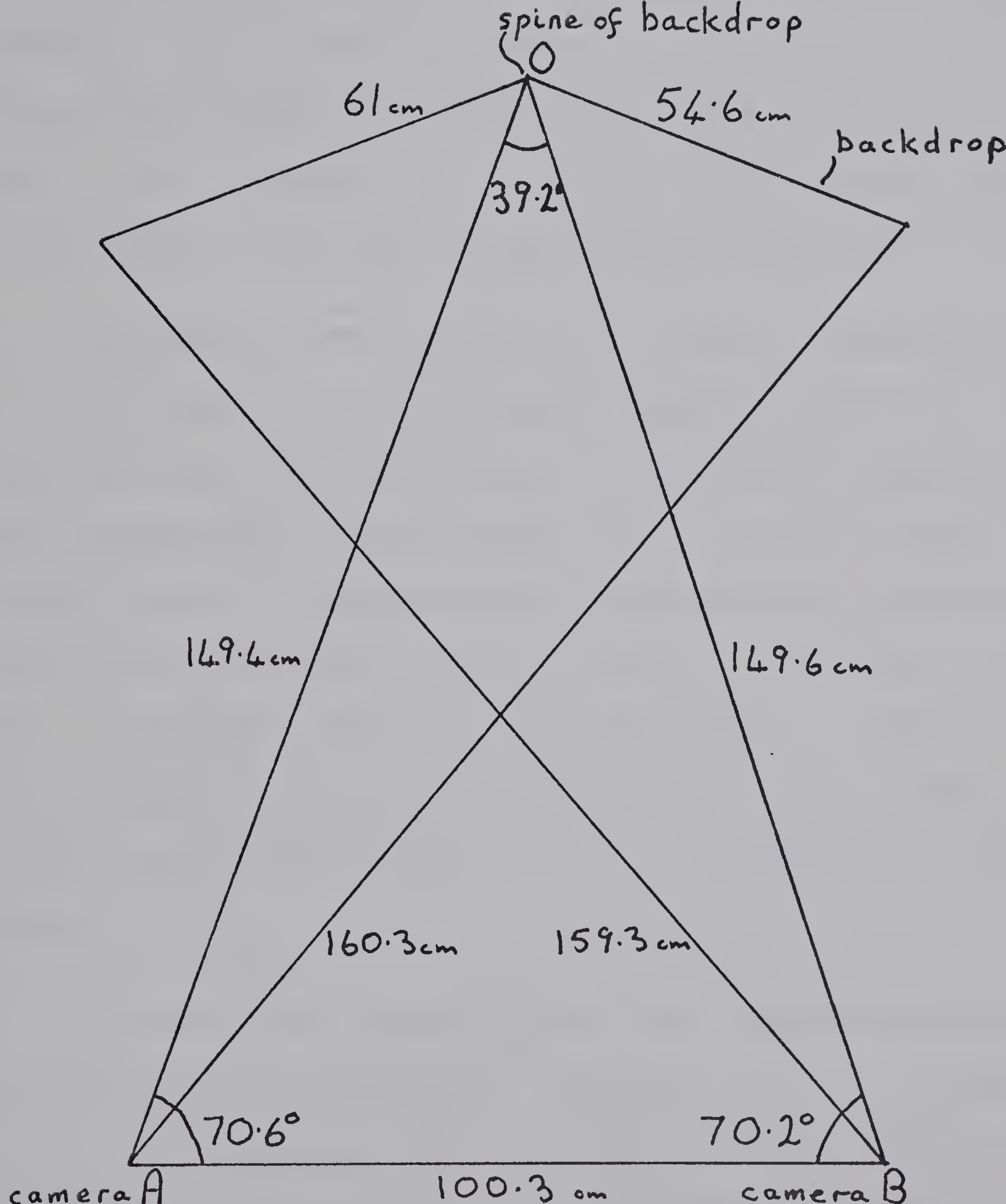

Figure 1. Plan view of the photographic arrangement.

arrangement (such as the van being parked on a slope) are discussed in Chapter 3.

The illumination necessary to obtain instantaneous hailstone images was supplied by two General Radio Strobolume light units which were mounted between the two cameras. The strobes were slaved and fired at a nominal 70 flashes per second, the actual flash rate, on calibration, being 70.2 flashes per second. This flash rate was independent of the power output of the generator.

The cameras were operated at a framing frequency of one or two per second, with a shutter speed of 1/8 or 1/15 s depending on the conditions. The film advance motors of both cameras were synchronized to a single timer which ensured that the cameras were taking virtually simultaneous photographs although it did not ensure that both shutters were released precisely simultaneously. Exact shutter synchronization was not generally critical as intense images arising from strobe flashes will be simultaneous on both films.

In order to avoid significant image blurring for a typical falling hailstone an exposure time of less than 100 μs is required, and in order to obtain more than two successive images of the same hailstone a flashing rate greater than 20 per second would be needed. These criteria are effectively met using the strobes, as their flashes have an exposure time of 12 μs, being the time for which the

light intensity is greater than one third of its peak value, and a repetition rate of 70.2 per second. For analysis there is the added convenience that successive images of a single hailstone are on the same photographic frame. Using this system, however, useful films were only obtained when the strobe illumination was sufficiently intense compared to the ambient daylight, to produce images that were much more intense than the streaks produced by the hailstones under the continuous ambient lighting. It was convenient to have a little ambient lighting as this produced faint streaks connecting the sharp images, thus identifying the successive positions of a single hailstone unambiguously. Under bright conditions only the streaks were observed. An example of the most useful film which was obtained is shown in Plate 3. One drawback of this multiple exposure technique is that although hailstone images are sharp in outline, when in focus, they lack surface detail.

Tri-X (400 ASA) negative film was used in 33 foot lengths, giving 250 exposures and a continuous filming time of 125 to 250 s, though it was generally fired in short bursts of about 10 to 15 s.

While photography was under way, the hail falling at the base of the backdrop was collected in a sawdust-filled box. Generally the stones collected, even over a minute or less, were too numerous and similar in structure to permit individual matching with images on the films and this

Plate 3. A sample of the hail film.
Frame 37 taken by camera A on August 7, 1974.

limited the usefulness of this exercise to the comparison of the statistical parameters of the film images to those of the collected stones.

2.4 Film Data Collected.

Filming was undertaken in several hailstorms, during July and August 1974, producing hail of all sizes up to golfball. Much of the film taken was capable of yielding some useful information but only on 8 days were good exposures with sharp hailstone images obtained. On 4 of these days the films show good multiple images (generally 4 images per stone) for several stones.

The most extensive film data obtained was that of August 7, which shows many distinct multiple hailstone images connected by faint streaks. The August 7 data consists of a continuous sequence of 65 frames, shot during a storm producing pea-size hail, at a location a few miles west of Ponoka (NE quarter, section 12, township 43, range 28 west of the 4th meridian).

The largest hail which was observed and filmed occurred on August 18. That storm was intercepted at three locations, near Spruceview, Bowden and Torrington respectively. The largest hail was walnut-size at the first and third locations and golfball-size at the second. Unfortunately this storm was intercepted under sufficiently bright conditions to render much of the film overexposed. A

short length of film showed clear multiple images and this was studied along with the August 7 data.

In view of the wealth of data, it was decided to concentrate the analysis on the film from the August 7 storm.

Chapter 3. FILM ANALYSIS.

3.1 The Measured Parameters.

In the course of this study the characteristics of hailstones which were under observation were size, shape, terminal velocity and rotation rate in free fall. Shape and rotation rate, for any stone for which sharp images were available on film, could be determined by direct observation of the projected film. The dimensions of hailstones and their trajectories could be accurately determined by making quantitative measurements of the dimensions and positions of successive images of the stones on film. The methods by which this three-dimensional information is obtained from the photographic data are described in the following sections of this chapter, as no previous report of this theory having been worked out in general has been found.

3.2 Relations between Film Images and Object Positions.

It is convenient, for subsequent calculations, to consider all three-dimensionally specified positions of hailstones in a right-handed coordinate system with the positive Z direction vertically downwards. Such a system is conveniently defined, for the case where the camera system was set up precisely as designed (Figure 1), as having the origin at O, the point of intersection of the optic axes of the cameras, and the positive Y-axis along the horizontal

line OA. In order to interpret film taken under field conditions it is necessary to consider the more general case where the two cameras were not necessarily directed horizontally or even at the same inclination to the horizontal, and the two optic axes did not intersect. These problems are discussed in sections 3.4 and 3.5. For this general case, a coordinate system is defined where the origin, O, lies on the optic axis of camera A at the point where this is intersected by a vertical plane containing the optic axis of camera B. The Y-axis lies along the vertical projection of the optic axis of camera A onto the horizontal plane through O; the Z-axis is vertical (positive downwards) and hence the positive X-axis points horizontally to the right, as viewed by camera A. It is convenient to designate measurements made in this reference frame by the subscript 'a' and measurements made in a similar frame attached to the optic axis of camera B by the subscript 'b'. However, up to section 3.3 the subscripts are omitted since the discussion applies equally validly to either frame so long as the two systems (a,b) are treated independently.

In order to relate the coordinates of an image point on film to the coordinates of the corresponding point in space it is necessary to consider three related rectangular coordinate systems, XYZ, X'Y'Z' and X"Y"Z" as shown in Figure 2. The XYZ system is the reference frame defined above. The X"Y"Z" system has the same origin and X-axis as the XYZ system but is rotated about the X-axis through an

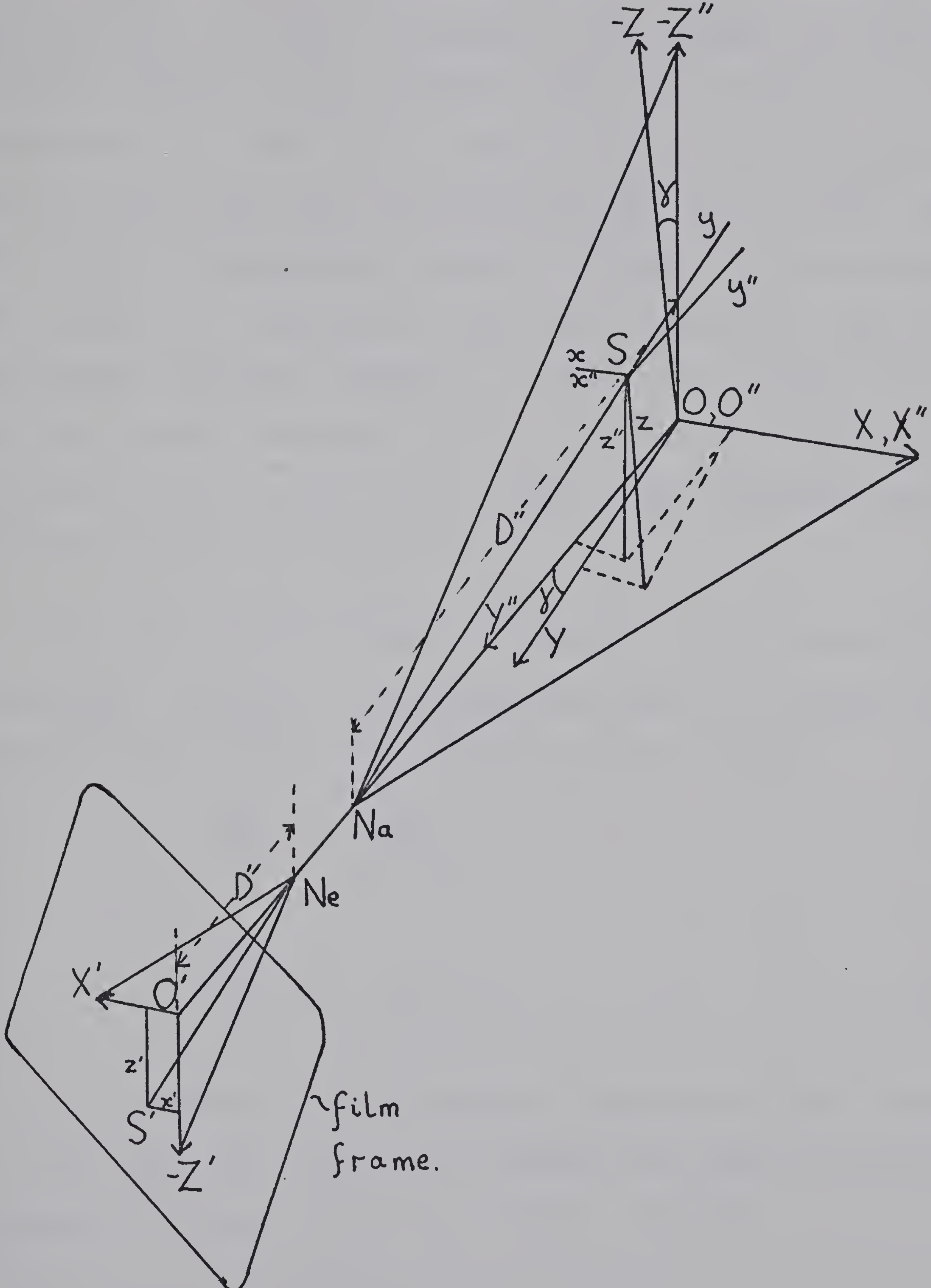

Figure 2. Relationship of spatial and film coordinate systems.

angle γ so that the Y"-axis lies along the optic axis of the camera. The X'Y'Z' system is defined such that the X'Z' plane is the camera's film plane, its origin, O', lies on the optic axis of the camera and the Z'-axis is the intersection of the film plane with the plane containing both the optic axis and the true vertical (the Z-axis). The other points of importance marked in Figure 2 are the camera lens's nodes of admission (Na) and emergence (Ne), an arbitrarily situated object, S, and its film image, S'. S is at the point defined by the coordinates (x,y,z) or (x",y",z") and S' is at (x',0,z'). The distance O'Ne is called D' and ONa is called D".

Mack and Martin (1939) presented the geometrical expressions relating to the magnification of a camera lens and from these we have the following relationships,

$$\frac{x'}{D'} = \frac{x''}{D''-y''} \tag{6}$$

$$\frac{z'}{D'} = \frac{z''}{D''-y''} \tag{7}$$

It is also evident, by considering a rotation of axes about OX, that the XYZ and X"Y"Z" frames have their respective coordinates for the point S related as follows,

$$x'' = x \tag{8}$$

$$y'' = y \cos\gamma - z \sin\gamma \tag{9}$$

$$z'' = y \sin\gamma + z \cos\gamma \tag{10}$$

Combining these two sets of equations we get the desired relationships between film coordinates and spatial coordinates:

$$x' = \frac{x D'}{D'' - y \cos\gamma + z \sin\gamma} \tag{11}$$

$$z' = \frac{(y \sin\gamma + z \cos\gamma) D'}{D'' - y \cos\gamma + z \sin\gamma} \tag{12}$$

In order to solve equations 11 and 12 for x and z it is necessary to know y; this is found by using data from both films of the stereo pair. The method is discussed in section 3.4.

Other authors have managed to obtain their desired information from a single camera either by restricting their studies to motion in two dimensions (Quick, 1974) or by determining y from the density, as measured by a microdensitometer, of the particle's image on film (Cannon, 1974). The latter method provides two different values for y which is a problem that would be a serious drawback in a study of particle kinematics but which can be easily overcome when studying only particle sizes since the

two values of y correspond to locations that are out of focus on opposite sides of the well-focussed volume. When a focussing correction is made, the dimensions of images at both locations are the same.

3.3 Projection and Measurement of Film Images.

In order to use measurements made from the film it is necessary to know the value of D' and D". In order to calculate D", it is also necessary to determine the separation distance, c, of the lens nodes Ne, Na. D' was calculated using the lens formula,

$$\frac{1}{D'} + \frac{1}{u} = \frac{1}{f} \tag{13}$$

where u is the distance from Na to the point at which the lens is sharply focussed and f is the focal length of the lens. This yielded D'=1.13 inches =28.7 mm, for u=46 inches, the distance at which both the lenses were focussed during the field experiment. Though the measurement of u may be slightly out it is certainly accurate to within ±4 inches, the error which would be required to alter D' at the accuracy quoted. In order to determine c, a grid of measured spacing was photographed at a known distance from the film plane, but with D' kept constant, and the resultant grid spacings on film were measured. Denoting the distance from the grid to the film plane by S we have

$$D'' - y = S - D' - c \tag{14}$$

and inserting this in equation 6 (since $\gamma = 0$, for this case) we can solve for c. This gives c=1.69 inches =42.9 mm.

In order to measure the film image coordinates (x',z') the films were projected on to a glass screen using a Recordak C-1 35 mm Film Reader. This allowed magnification of up to 20 times the original film size. The distortion of the picture due to the camera and projector lenses was very small, the maximum error, from this cause, in a position measurement being 1.6%. This was determined by measuring the variations, over the field of view, in the spacing of a square grid projected by the film reader, and then projecting, using the same reader, a photograph of a square grid, taken using one of the cameras used for the field study. Errors from this cause were kept ten times smaller by arranging the projection so as to avoid using the extreme corners of the projection screen.

The coordinates of the apparent centres of hailstone images were taken as being midway between the extremes (both horizontally and vertically) of the image. Other methods of defining the centre would be unlikely to reduce the errors involved. The coordinates of the hailstone centres were measured by placing a transparent overlay with a 0.1 inch grid over the screen. This grid was centred for convenience

at a mark on the backdrop (appearing in every frame) which was near the origin, O'. The grid was aligned with the direction of the Z'-axis, defined, for any sequence of photos, by the mean direction of the plumb line in the sequence. It was necessary to take the mean plumb line position as the instantaneous position of the plumb line varied from picture to picture, oscillating through a small angle about a well defined mean position. The position of the origin, O', the centre of the photo-frame was noted as the point of intersection of the diagonals. The coordinates which were measured off the grid (x"',z"') were hence readily referred to the optic axis. These coordinates were measured to an accuracy of 0.02 inch. The true film coordinates, x',z', as used in equations 11 and 12, are simply these measured values (x"',z"') divided by the magnification ratio of the projector. The measurement error in x',z' is hence 0.001 inch (0.025 mm).

3.4 Calculation of Three-dimensional Hailstone Positions.

In order to determine the spatial coordinates of any point, such as a hailstone's apparent centre, it is necessary to measure the film coordinates of the apparent centres of corresponding images on both films (x_a', z_a', x_b', z_b'). These two apparent centres may not be precisely the same point in space and allowance for this is made later. It is also necessary to consider the relationship of the two reference frames $X_aY_aZ_a$ and $X_bY_bZ_b$ as shown, for a

general case, in Figure 3. The origin of the $X_a Y_a Z_a$ frame is at O; the origin of the $X_b Y_b Z_b$ frame, as it was discussed in section 3.2, is at the point marked R. However, the $X_b Y_b Z_b$ axes have been translated vertically by a distance RO, which will be denoted by d, so that both reference frames now have a common origin at O. The only alteration this makes to the equations already derived is that where z_b appears it is replaced by $z_b - d$.

The 'baseline', defined to be the separation of the nodes of admission (Na) of the lenses of the two cameras, is assumed to make an angle γ_c with a horizontal plane. The optic axes are tilted by γ_a and γ_b with respect to their vertical projections onto the horizontal plane, the Y_a and Y_b axes. These axes are separated by an angle β. Y_a and Y_b make angles α_a and α_b with the vertical projection of the baseline onto the horizontal plane. All these parameters are constants for any particular situation, i.e. for one filming sequence, and, though they will be determined later, may be assumed at this stage to be known constants.

With the film coordinates (x_a', z_a', x_b', z_b') measurable, it is now possible to determine the spatial coordinates, (x_a, y_a, z_a) or (x_b, y_b, z_b), of a particular hailstone image. The coordinates in the two frames, 'a' and 'b', are related, through rotation about the common Z-axis, by the equations,

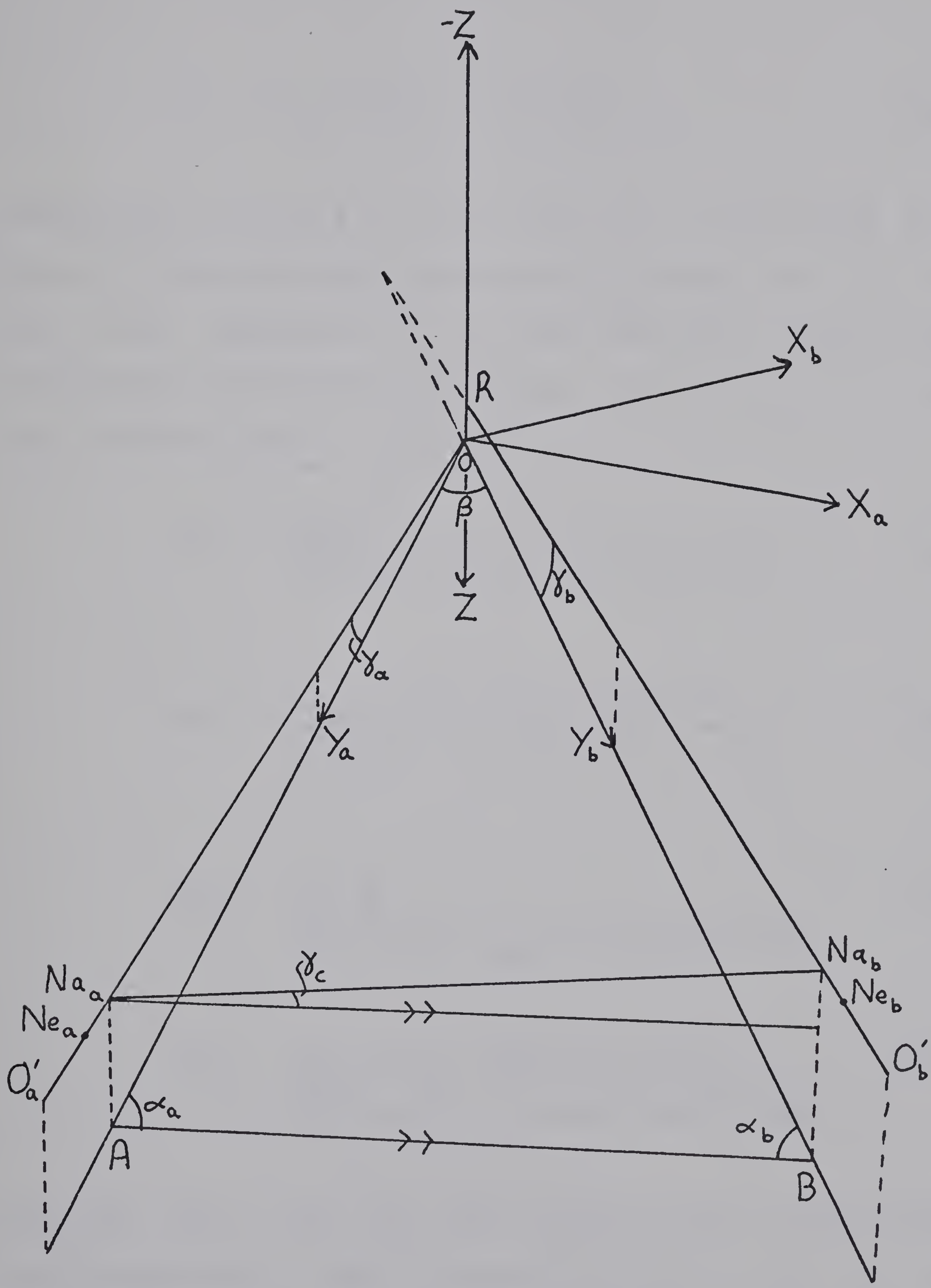

Figure 3. Relationship of spatial reference frames. The triangle OAB defines a horizontal plane while OZ, ANa_a and BNa_b are all vertical lines.

$$x_a = y_b \sin\beta + x_b \cos\beta \tag{15}$$

$$y_a = y_b \cos\beta - x_b \sin\beta \tag{16}$$

Substituting $D_a/\cos\gamma_a$ for D_a'' where D_a is the length OA in Figure 3, and similarly substituting $D_b/\cos\gamma_b$ for D_b'', we have, from equations 11, 12, four equations relating film coordinates and spatial coordinates. Noting that D' is the same for both cameras, these are

$$x_a' = \frac{x_a D'}{D_a/\cos\gamma_a - y_a\cos\gamma_a + z_a\sin\gamma_a} \tag{11a}$$

$$z_a' = \frac{(y_a \sin\gamma_a + z_a\cos\gamma_a)D'}{D_a/\cos\gamma_a - y_a\cos\gamma_a + z_a\sin\gamma_a} \tag{12a}$$

$$x_b' = \frac{x_b D'}{D_b/\cos\gamma_b - y_b\cos\gamma_b + (z_b-d)\sin\gamma_b} \tag{11b}$$

$$z_b' = \frac{(y_b\sin\gamma_b + (z_b-d)\cos\gamma_b)D'}{D_b/\cos\gamma_b - y_b\cos\gamma_b + (z_b-d)\sin\gamma_b} \tag{12b}$$

Equations 11a, 12a, 11b, 12b, 15 and 16 are 6 simultaneous linear equations in the 6 unknowns, x_a, y_a, z_a, x_b, y_b and z_b, and hence they can be solved to give the spatial coordinates in terms of the constants and measurable

quantities. The solutions providing (x_a, y_a, z_a) are given by

$$z_a = \frac{R_a + S_a\left(\dfrac{z_a' \, D_a/\cos\gamma_a}{D'\sin\gamma_a + z_a'\cos\gamma_a}\right)}{T_a + S_a\left(\dfrac{D'\cos\gamma_a - z_a'\sin\gamma_a}{D'\sin\gamma_a + z_a'\cos\gamma_a}\right)} \qquad (17)$$

where
$$R_a = \frac{D_a}{\cos\gamma_a} x_a' \left\{ x_b' \sin\beta + \cos\beta\left(D'\cos\gamma_b - z_b'\sin\gamma_b\right)\right\} - D_b \, x_b' \, D'$$

$$S_a = z_b' \sin\gamma_b \left(D'\sin\beta + x_a'\cos\gamma_a\cos\beta\right) + x_a'\cos\gamma_a\left(D'\cos\gamma_b\cos\beta - x_b'\sin\beta\right) + x_b' D'\cos\beta - D' D'\sin\beta\cos\gamma_b$$

$$T_a = x_a' \sin\gamma_a \left\{\cos\beta\left(z_b'\sin\gamma_b - D'\cos\gamma_b\right) - x_b'\sin\beta\right\}$$

$$y_a = \frac{z_a' D_a/\cos\gamma_a + z_a\left\{z_a'\sin\gamma_a - D'\cos\gamma_a\right\}}{D'\sin\gamma_a + z_a'\cos\gamma_a} \qquad (18)$$

$$x_a = \left(y_a\sin\gamma_a + z_a\cos\gamma_a\right) x_a'/z_a' \qquad (19).$$

The solutions providing (x_b, y_b, z_b) are given by

$$z_b - d = \frac{R_b + S_b\left(\dfrac{z_b' \, D_b/\cos\gamma_b}{D'\sin\gamma_b + z_b'\cos\gamma_b}\right)}{T_b + S_b\left(\dfrac{D'\cos\gamma_b - z_b'\sin\gamma_b}{D'\sin\gamma_b + z_b'\cos\gamma_b}\right)} \qquad (20)$$

where $$R_b = \frac{D_b}{\cos\gamma_b} x_b' \left\{ x_a' \sin\beta + \cos\beta \left(z_a' \sin\gamma_a - D' \cos\gamma_a \right) \right\} + D_a x_a' D'$$

$$S_b = z_a' \sin\gamma_a \left(D' \sin\beta - x_b' \cos\gamma_b \cos\beta \right) + x_b' \cos\gamma_b \left(D' \cos\gamma_a \cos\beta - x_a' \sin\beta \right) - x_a' D' \cos\beta - D' D' \sin\beta \cos\gamma_a$$

$$T_b = x_b' \sin\gamma_b \left\{ \cos\beta \left(D' \cos\gamma_a - z_a' \sin\gamma_a \right) - x_a' \sin\beta \right\}$$

$$y_b = \frac{z_b' D_b / \cos\gamma_b + (z_b - d)\left\{ z_b' \sin\gamma_b - D' \cos\gamma_b \right\}}{D' \sin\gamma_b + z_b' \cos\gamma_b} \qquad (21)$$

$$x_b = \left(y_b \sin\gamma_b + (z_b - d) \cos\gamma_b \right) x_b' / z_b' \qquad (22).$$

Taking measurements of the positions of the simultaneous 'a' and 'b' images of a single hailstone and using equation 17 to evaluate z_a and equation 20 to evaluate z_b, the values of z_a and z_b should be identical, to within the errors of measurement which are discussed later in this section. This provides an objective method of determining which photographic images are true pairs corresponding to a single hailstone. On any photograph, successive images of a single stone can generally be identified by faint connecting streaks caused by continuous ambient lighting. It is thus fairly simple to measure the coordinates on a frame from either camera of successive photographic images of the same

stone, and generally this can be done for several stones in the same frame. The next step is to pair the image coordinates of each stone from an 'a' frame, in turn, with those of each stone from the simultaneous 'b' frame and, for each image pair calculate z_a and z_b. For most of these pairings z_a and z_b will not be equal but for a few (a maximum of one per stone) we have $z_a=z_b$, to within an acceptable error. These may be expected to be true pairs of images of the same stone. The acceptable difference between z_a and z_b was taken as 1 cm. This allows for discrepencies that may arise due to measurement errors of up to 0.02 inch (0.05 cm) in the measured film coordinates (x''', z'''), giving resultant errors up to 0.15 cm in the spatial coordinates, and an error of similar magnitude arising, for non-spherical stones, from the apparent centre being at a slightly different spatial position for different viewing angles. The acceptable difference of 1 cm is also sufficient to allow for slight discrepancies in coordinate calculations arising from errors in calculating the camera orientation parameters (angles and distances) as these discrepencies were less than 0.2 cm. This criterion appeared to successfully select true pairings and to eliminate incorrect pairings as most pairings that were rejected had a difference of far greater than 1 cm between z_a and z_b. In addition, most of the pairings that were accepted as true were pairings that seemed probable from visual inspection of the photographs.

3.5 Calculation of Camera Orientation Parameters.

In order to use the method discussed in section 3.4 to determine spatial coordinates, it is necessary to evaluate the changeable parameters which were taken as constants in deriving equations 17 to 22. These are D_a, D_b, β, γ_a, γ_b, and d. The main variations in the parameters, from one film sequence to another, arise from the van having been parked on ground of different gradient on each occasion. A smaller variation arose because each camera was mounted by a conventional tripod clamping screw, and hence could rotate slightly about a quasi-horizontal axis, lying parallel to its film plane. This effect produced farther variations in γ_a and γ_b and made d non-zero. It is possible that the cameras would also move slightly owing to their mountings being 'sprung' for shock absorption.

Considering the horizontal triangle OAB in Figure 3, it can be seen that

$$D_a = AB \sin \alpha_b / \sin \beta \tag{23}$$

and

$$D_b = AB \sin \alpha_a / \sin \beta \tag{24}$$

When the camera lenses' nodes are at the same level and in the configuration of Figure 1, the separation of the lenses' nodes of admission, $Na_a Na_b$, is 95.3 cm. The tilt of the van, γ_c , is included in the calculations in order to

evaluate the distance AB (Figure 3) in a particular instance since it gives us

$$AB = 95.3 \cos \gamma_c \qquad (25).$$

It is now seen that the changeable parameters, D_a, D_b, β, γ_a, γ_b, and d, can all be expressed in terms of d and the six angles α_a, α_b, β, γ_a, γ_b and γ_c, since D_a is a function of α_b, β and γ_c and D_b is a function of α_a, β and γ_c. The six angles are not independent since $\alpha_a + \alpha_b + \beta = 180°$.

In order to determine the values of the angles, equations 17, 18 and 19 were used, to determine the coordinates of string crossing points on the backdrop grid. Grid point coordinates, for several neighbouring points on the backdrop were measured from a stereo pair of frames from the film sequence under study. Each of the angles α_b, β, γ_a, γ_b, γ_c was varied in turn over a physically reasonable range and, for each set of values, equations 17, 18 and 19 were used to evaluate the grid point coordinates and hence the grid point spacing (which was 10 cm). The values of the angles which minimised the errors in evaluating the grid point spacing were selected. The value of d was then chosen so as to minimise the difference between z_a and z_b for the points which had been used to determine the angles. That the selected parameters provided a small difference between z_a and z_b for points away from the backdrop, was checked by measuring the positions of hailstone images which could be

paired unambiguously, such as the images of a stone which had ricocheted off the side of the van. The camera orientation parameters thus obtained for the cases studied are given in Table 1.

Once these parameters have been determined for a particular film sequence, equations 17, 18, 19 and 20 may be used to identify true pairs of hailstone images, and determine the spatial coordinates of the successive images of these hailstones, for all frames in that sequence. Once these spatial coordinates have been obtained, it is convenient to work entirely in the 'a' frame and drop the subscript 'a' so that the quantities calculated as x_a, y_a, z_a will now be referred to as x, y, z.

3.6 Calculation of Hailstone Dimensions.

It is necessary in a study of this nature to know the sizes, and the shapes, of the hailstones for which data is collected. Apart from a qualitative observation of shape, the measurements used in this study are the maximum and minimum diameters (this term being used synonymously with 'dimensions') visible to the camera from whose film measurements are made (generally 'a'). The ratio of these values gives a measure of the non-circularity of the hailstone image, and the values themselves give the stone size.

For each stone, for which unambiguous spatial

Table 1.

Camera orientation parameters for selected film sequences.

Parameter.	Film sequence.	
	August 7	August 18
α_a	70.8°	70.8°
α_b	70.2°	69.0°
β	39.0°	40.2°
γ_a	-1.4°	0.1°
γ_b	2.0°	0.7°
γ_c	5.0°	2.5°
d	1.31 cm	1.17 cm
AB	94.9 cm	95.2 cm
D_a	141.9 cm	137.7 cm
D_b	142.5 cm	139.3 cm
D_a''	142.0 cm	137.7 cm
D_b''	142.5 cm	139.3 cm

coordinates have been obtained, the major and minor apparent diameters (i.e. the greatest and least dimensions visible to the camera) of an image on the 'a' frame are measured, and from these the corresponding dimensions of the stone can be calculated. If all points in the camera's field of view were perfectly in focus simultaneously then we would simply have

$$\delta = \frac{\delta'}{D'}\left(D_a'' - y\cos\gamma_a\right) \tag{26}$$

where δ is the hailstone diameter and δ' is the diameter measured on the film. However, the size of the photographic image of a hailstone is increased by the diameter of the 'circle of confusion', which has a non-zero value for all points not at the distance from the lens at which the lens is perfectly focussed (Mack and Martin, 1939). The circle of confusion (i.e. the amount by which any measured film diameter is too great) is given by

$$c = \left|\frac{D'f}{u} - D' + f\right|\left(\frac{a}{f}\right) \tag{27}$$

where D' and f (the focal length of the lens) are as before, $u = D_a'' - \cos\gamma_a$, and a is the diameter of the lens aperture. Since the lens's f-number is simply f/a and the lenses were used at their maximum aperture (given by f/3.5), equation 27 becomes, for the lenses used in this study,

$$c = \left|\frac{D'f}{u} - D' + f\right| / 3.5 \tag{28}$$

In practice it may be that image intensity drops off

sufficiently towards the edge of an image to cause only a portion of the calculated circle of confusion, say p ($0<p\leq 1$), to be in fact observed. Applying this as a correction to equation 26 we get an expression for a hailstone's diameter (δ) in terms of measured parameters:

$$\delta = (\delta' - pc)\, u / D' \qquad (29).$$

For a large sample of hailstones it should be possible to determine p by chosing the value which gives a stone size distribution, from the films, which most closely matches that determined independently from a sample of hailstones collected at the time of the filming.

3.7 Determination of Terminal Velocities.

The calculations discussed in the preceeding sections provide coordinates of hailstone images at equal time intervals of 14.2 ms, the time between successive strobe flashes. From this data the vertical and horizontal components of the hailstone's velocity may be readily determined.

Being interested in terminal velocities, it is first necessary to eliminate those stones which are still accelerating, such as the stones which appear to have bounced off the roof of the van. This is readily done as the vertical spacing of their images increases monotonically with time.

For the remaining hailstones, mean velocity components and deviations from the mean, both in the vertical and horizontal, are derived by calculating the mean component for each 1/70.2 s interval between successive hailstone images. For example, if the mean vertical fallspeed and its RMS variation are desired for a stone producing four images on film, which we denote by subscripts, they are given as follows, where coordinates are in cm and speeds in ms^{-1}.

Mean vertical fallspeed = $w_0 = 0.702(z_4 - z_1)/3$

RMS variation = $[\{(w_1 - w_0)^2 + (w_2 - w_0)^2 + (w_3 - w_0)^2\}/3]$

where $w_1 = 0.702(z_2 - z_1)$

$w_2 = 0.702(z_3 - z_2)$

$w_3 = 0.702(z_4 - z_3)$.

Similar calculations produce the mean horizontal components of the stone's velocity, and deviations from that mean. In practice use was only made of the mean velocity measurements as the RMS variation was of the same order of magnitude, and so probably largely due to, measurement errors.

3.8 The Study of Rotation Rates.

It was originally hoped that a detailed quantitative study of rotation rates could be made by observing the motion of individual surface features of each stone. However, the film obtained from the field experiment was taken under such lighting conditions that surface features were not visible on stones and even distinct lobes were

often difficult to identify on successive images.

The only direct observations of rotation that could be made were the apparent change in orientation of non-spherical stones in successive locations, and the variation in the width of continuous fallstreaks due to the rotation of non-spherical stones. This method depends on a stone being distinctly non-spherical in order that its rotation or oscillation can be observed directly and so little direct information can be obtained in this way about near-spherical stones or stones which have an axis of rotational symmetry which is also their axis of rotation.

Chapter 4. RESULTS.

4.1 Hailstone Size Distribution.

In order to determine the dimensions of the hailstones, which were observed in free-fall, it was necessary to determine the portion of the circle of confusion which was observed in each hailstone image, as described in section 3.6. This was done by comparing the size distribution of the hailstone images measured from the film of August 7 with the size distribution of a sample of hailstones collected over a five minute period, during which filming lasted for 30 seconds. This size distribution was measured independently.

As in the remainder of this discussion, August 7, 1974 was the main case under study, data for 55 stones being measured on film. Where appropriate, reference is also made to the film data collected on August 18, consisting of successive position coordinates for the 5 stones which were identified. It should again be noted that the hailstones being discussed here are smaller than those discussed by most previous authors. The 5 stones of the August 18 sample and 42 of the stones in the August 7 sample were true hail (i.e. they had a maximum diameter greater than 5 mm). The remaining 13 stones observed on August 7 were ice pellets. The smaller stones were probably not snow pellets because a sample of the stones collected in cold hexane appeared to be

entirely ice pellets; i.e. they did not have the low density characteristics of snow pellets.

Since no stones with a maximum diameter (diameter being taken as any linear dimension) greater than 1.0 cm were identified on the August 7 films, the frequency distribution of maximum diameters in 1 mm intervals, up to this limit, was determined. The independent sample of stones was spread on a dark cloth, along with a scale, and photographed. Measurements of hailstone diameters were made from this photograph. Size distributions, for ten different values of p, the proportion of the circle of confusion allowed for, from 0.1 to 1.0, were calculated from the data measured off the film of August 7 using equation 29.

Each of these calculated size distributions was compared in turn with the independent sample using a chi-squared test. As both samples were small, for use with this test, and were not necessarily close enough to a normal distribution for the test to be reliable, the best fit was significant at a level of less than 1%. The test did show that the best fit was obtained for p=0.6, i.e. allowing for 60% of the circle of confusion being visible on the images of out of focus stones. Since little confidence can be placed on this choice of p, it is important to take account of the errors that would arise from an incorrect choice of p.

In calculating the dimensions of hailstones, this value

of p was used so that equation 29 becomes

$$\delta = (\delta' - 0.6c)\,u/D' \qquad (30).$$

It is likely that any error in this calculated value for p could result in considerable errors in measured hailstone diameters for images that are far out of focus. However, for most of the stones observed in this study, the maximum error in diameter measurement due to this cause was less than 1 mm, with 0.4 mm being typical. For example, if the maximum error were made in the choice of p (i.e. if p=0), diameters would only be in error by 1 mm for stones for which the calculated diameter of the circle of confusion was greater than 1.7 mm, and there were only 12 such stones. If the evaluation of p was in error by 0.2 then the typical error in observed hailstone diameters from this cause would be 0.2 mm. Though p may be a function of the radius of the circle of confusion, rather than a constant as chosen here, there was no method available to test this reliably in this case.

The hailstone size distribution obtained from the film data, with p=0.6, is shown as a histogram in Figure 4 along with the distribution obtained from a photograph of the independent sample. The cumulative distribution curves for the same cases are shown in Figure 5. The differences in detail between the two distributions are possibly due to short term variations in the distribution during the time taken to collect the independent sample, since the two

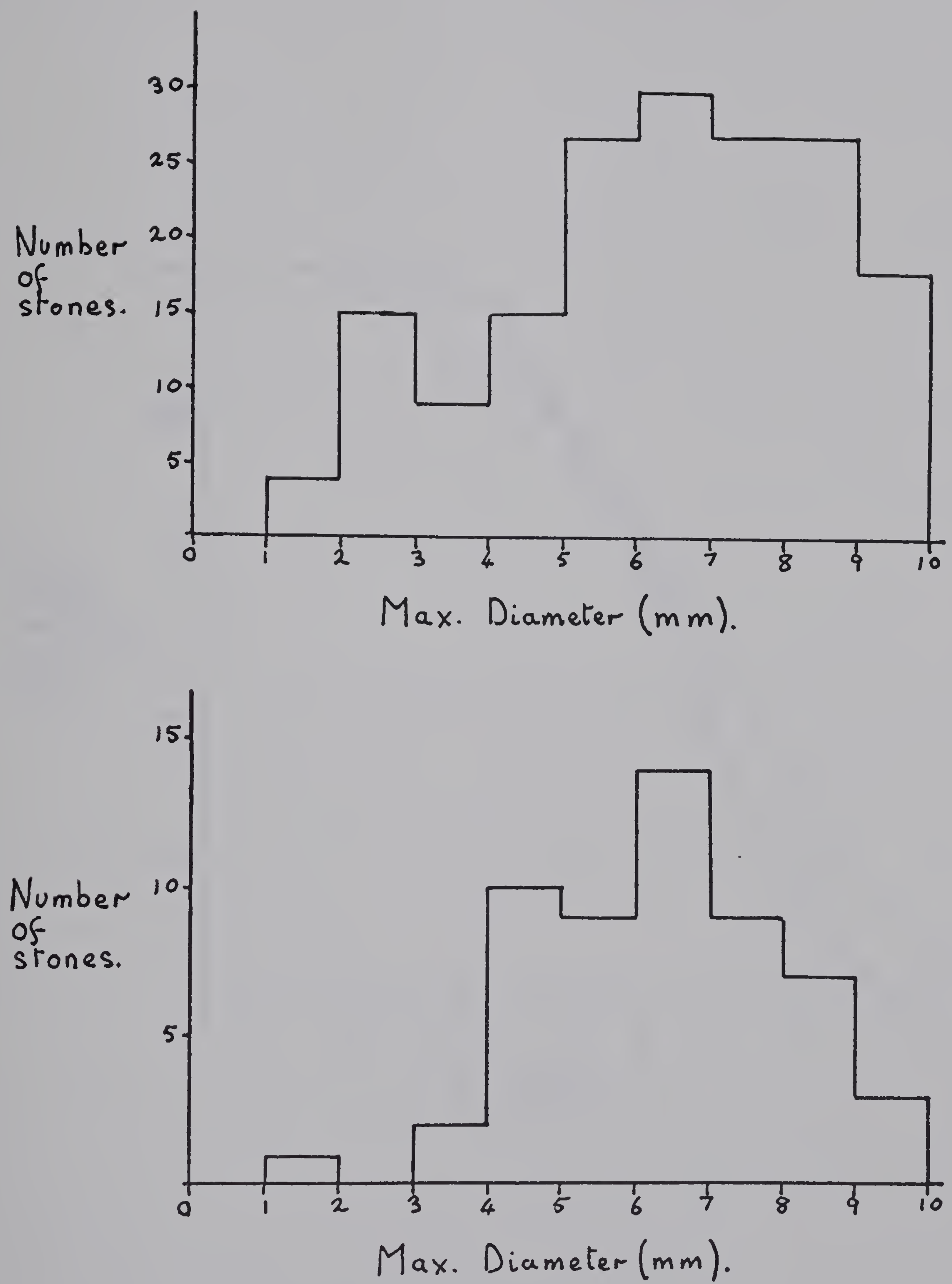

Figure 4. Hailstone size distribution observed on August 7. Independent sample (above) and filmed sample (below).

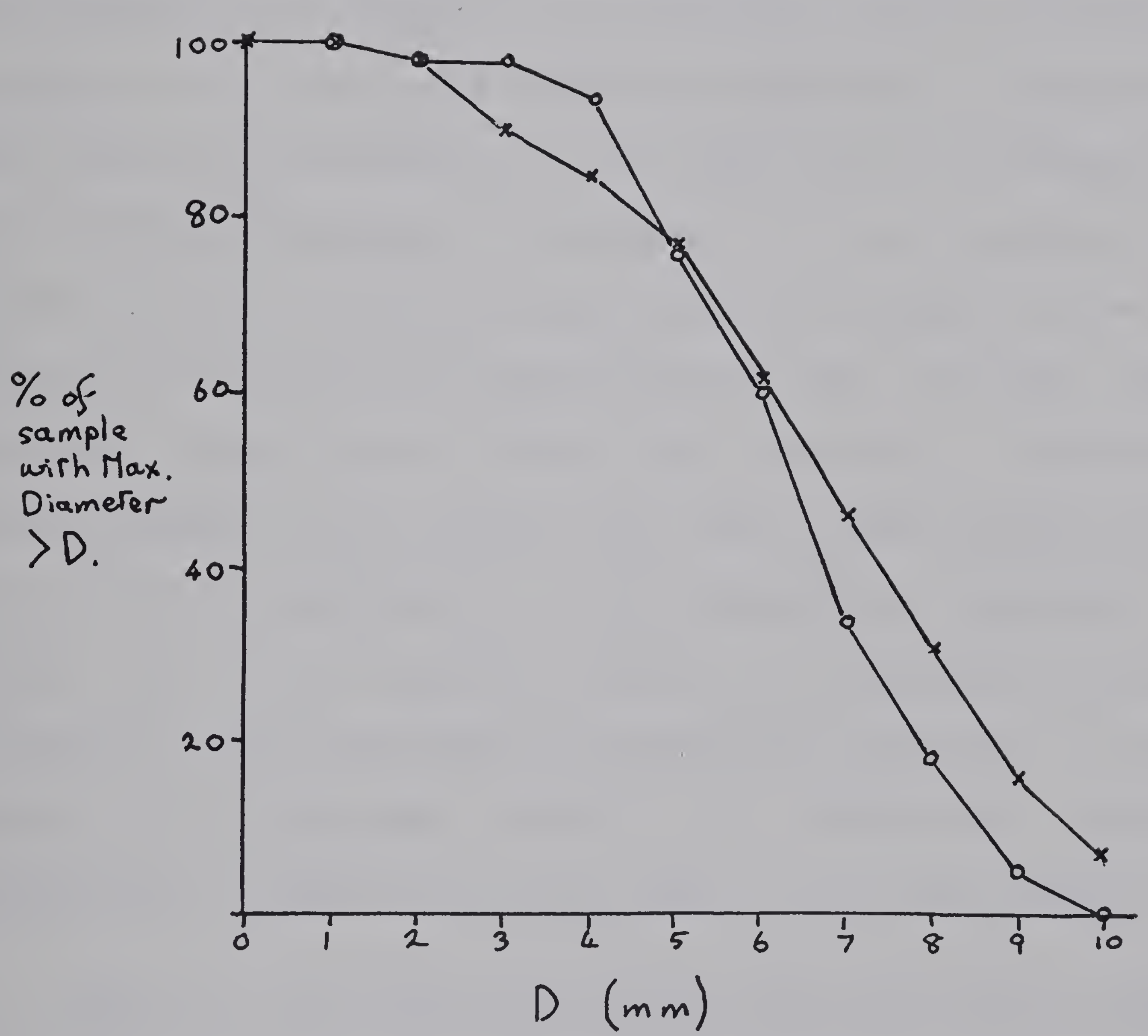

Figure 5. Cumulative hailstone size distribution observed on August 7 for the independent sample (denoted by x) and filmed sample (o).

samples were collected over different time intervals. This possibility enhances the view that consideration of the possible errors due to an erroneous p may be more significant than the evaluation of p itself.

The possible error in measuring the dimensions of hailstone images off projected films is 0.01 inch which corresponds to an error, at the distance of the backdrop, of 0.55mm in the calculated hailstone dimension. Combined with the error in the evaluation of p this gives a possible error of 0.75 mm in hailstone dimensions. It is unlikely that actual errors are this large since the larger of the above errors is evaluated for hailstones at the distance of the backdrop where such errors are greatest. However, for stones nearer to the camera than the in-focus region, as the error due to measurement of film dimensions decreases, the error due to an incorrect choice of p increases and so the composite error may remain approximately constant. For this reason the estimated error in calculated hailstone dimensions is taken to be the same for all data points.

Most of the hailstone images were distinctly observed to be non-spherical, the most common shapes approximating to cones and ellipsoids. The measurement that was made to take account of variation in shape was the axis ratio, the ratio of the minimum and maximum measured diameters (or linear dimensions) of a hailstone. The maximum error in this quantity was typically 25% as there was a maximum error of

0.75 mm in the measurement of each diameter and, for the August 7 sample, the mean minimum diameter was 4.6 mm while the mean maximum diameter was 6.3 mm. This gives a mean axis ratio of 0.73.

4.2 Accuracy of Fallspeed Measurements.

The major part of this study is concerned with the observation of hailstone fall velocities, and the accuracy of the resulting measurements is discussed in this section. Each component of the fall velocity can be measured with the same accuracy, as this is dependent only on the flash rate of the strobe lighting, and the error in measuring the coordinates of successive hailstone images.

Since the strobe flash rate was found to be constant to better than 0.1% and independent of generator speed or power output, errors from this source were ignored and the flash rate was taken to be precisely the measured value of 70.2 flashes per second.

For non-spherical stones it is possible that the apparent centre of a stone image is not the true centre of mass; an error of 0.02 inch in measuring the film coordinates of an image could arise from this cause. The film coordinates of a given point could be measured to within a further 0.02 inch. This results in a possible error of 0.04 inch in measuring the film coordinates of a hailstone's location. For points in space near the backdrop

this corresponds to a possible spatial error of 2.2 mm. The maximum possible error in measuring the separation of successive hailstone images is thus 4.4 mm. In calculating fallspeeds from successive images there is thus a possible error of 0.3 ms^{-1}. However measurements of the mean value of fall velocity components were generally taken from four successive hailstone images separated by three time intervals, each of 14.2 ms. For these calculations, the error in a velocity determination is reduced to 0.1 ms^{-1}. Therefore the major error in relating fallspeed to stone size is in the measurement of the hailstone size where, for smaller stones, errors of up to 15% may be expected.

For hailstones that were not continuously accelerating, the error in fallspeed measurement is of the same order of magnitude as observed velocity variations. Therefore it is not possible to calculate accurately the fallspeed fluctuations from the data obtained in this study.

The possible errors in the measured and calculated parameters relating to the hailstone images under study are summarised in Table 2.

4.3 Horizontal Components of the Fall Velocity.

The wind having a dominant influence on the horizontal components of a hailstone's motion, these components, measured for several stones during a short period of time, reflect the short term variations in the wind. Accordingly

Table 2.

Probable maximum errors
in hailstone dimensions and fallspeeds.

Quantity.	Error.
Hailstone diameter	
- due to measuring film images	0.55 mm
- due to incorrect allowance for circle confusion	0.20 mm
- composite	0.75 mm
Hailstone axis ratio	25%
Hailstone image location	2.2 mm
Hailstone image separation	4.4 mm
Velocity component	0.1 ms^{-1}

measures of the mean and fluctuating parts of the horizontal velocity components of the hailstones are measures of the corresponding properties of the wind. These horizontal velocity components were much larger than the horizontal components that could be induced by tumbling so if the latter are present they are masked.

For the hailstones observed on August 7 the mean horizontal component of velocity was 1.3 ms^{-1} with most of the hailstones having a horizontal velocity component within ±0.3 ms^{-1} of that value. For August 18 the horizontal velocity component was measured to be 7.0±1.5 ms^{-1}. Though this latter measurement is based on a small data sample, it is supported by the observation that in each film frame from which hailstones were identified there were several approximately parallel streaks, with images similarly spaced to those that were measured, indicating that many more stones had similar horizontal velocities. However, the stones giving most of these streaks did not give identifiable images on both films.

4.4 The Vertical Component of Terminal Velocity.

Authors in the past have concentrated their attention on obtaining an empirical relationship between a representative diameter of hailstones and their terminal velocities (e.g. Roos and Carte, 1973). In order to compare the results of this study with previous results, the

relationship between the vertical component of the measured velocity and the maximum observed diameter for the hailstones of August 7 will be illustrated.

Other authors' terminal fall velocity data are presented in Figure 6 which is adapted from Auer (1972). This data for graupel and hail extends over a greater size range than the data in this study. However, this is not all natural hail data as it includes the results of theoretical studies and experiments on models. The measurements presented in Figure 6 were made at a ground elevation of 7000 feet MSL (c. 2130 m). The curve shown along with this data is not a fit to the data but is given by equation 2 with ρ_a=0.99 kgm^{-3} (corresponding to a standard atmosphere at the elevation given above) and with C_D=0.6 and is included for comparison. Similar curves are included in subsequent graphs for comparison with the data obtained in this study. The drag coefficient value of 0.6 was chosen (after Roos and Carte, 1973; Strong, 1974) because the theory providing equation 2 assumes hailstones to be spheres. Smooth spheres have drag coefficients of about 0.45 whereas hailstone drag coefficients will be slightly greater due to the stones being rough and, in general, slightly flattened compared to spheres. C_D=0.6 is therefore chosen as a general value for hailstones though it does not necessarily apply to the stones of any particular sample. Figure 6 shows that equation 2 provides a rough estimate of hailstone fallspeeds though further factors must be

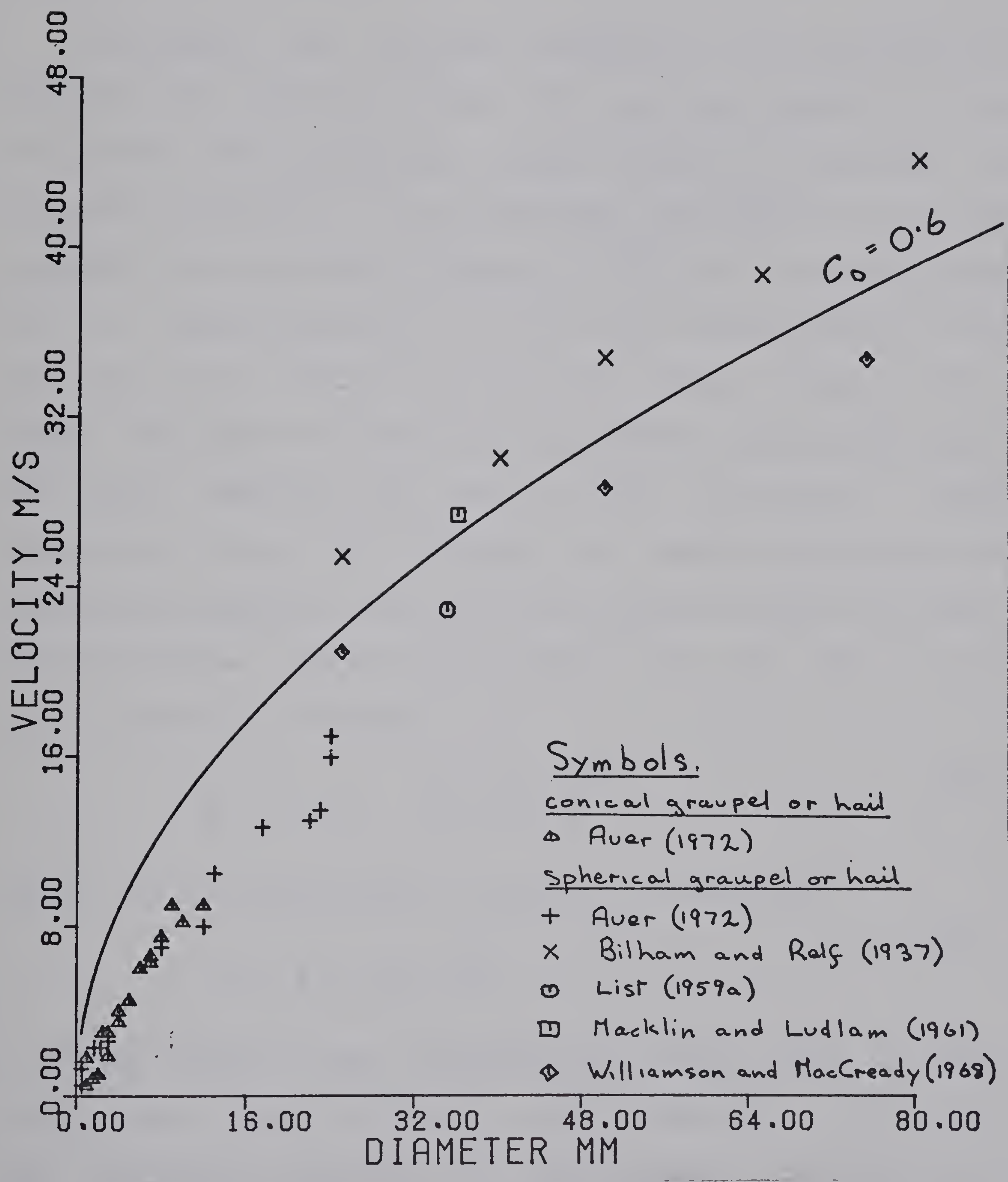

Figure 6. Observed and derived relationships between terminal fall velocity and diameter of graupel and hail (after Auer, 1972). A theoretical curve is given for comparison.

considered in order to obtain an accurate estimate. Five of the data sets illustrated in Figure 6 consisted of spherical hail; the sixth consisted of conical graupel and hail.

In Figure 7 the vertical component of the terminal velocity is plotted against the maximum diameter of the hailstones, with appropriate error bars as described in sections 4.1 and 4.2. For comparison, the plotted curve was obtained using equation 2 with $\rho_a = 1.09$ kgm^{-3} (corresponding to the ambient pressure of 912 mb and temperature of 19 C) and with C_D=0.6 (after Roos and Carte, 1973; Strong, 1974). Since the observed stones were apparently composed of solid ice their density was taken to be 0.89 gcm^{-3}. This illustrates that this formula is useful for most of the hailstones observed, provided that velocity errors of 2 ms^{-1} are acceptable. Where V is in ms^{-1}, D im cm, and ρ_a in kgm^{-3}, equation 2 becomes

$$V = 13.9 \; (D/\rho_a)^{1/2} \tag{31}$$

which, for the conditions of August 7, reduces to

$$V = 13.3 \; D^{1/2} \qquad (32),$$

a result close to that calculated by Strong (1974) for mean conditions in Central Alberta. This expression gives only the vertical component of the terminal velocity; the horizontal component however, being determined by the wind, can also be significant in contributing to the total impact energy of hailstones.

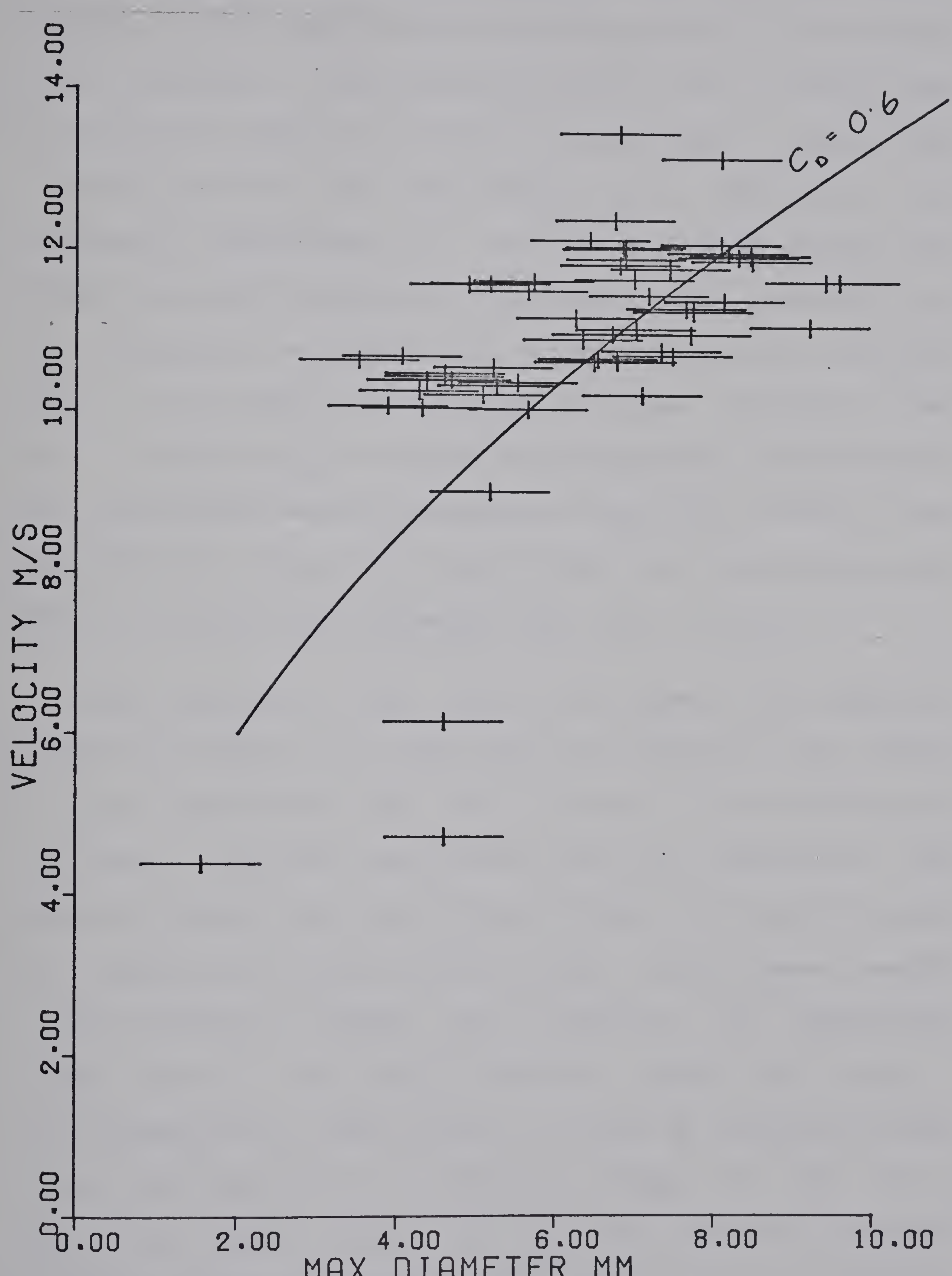

Figure 7. Vertical component of terminal velocity vs. maximum hailstone diameter for August 7 sample. The theoretical curve is given by equation 2.

It should be noted, however, that the velocities measured in this study were measured relative to the ground and not relative to the surrounding air. For a falling body to achieve its terminal velocity it must reach a stable mode of motion involving the surrounding air. As there were unmeasured fluctuations in the vertical wind field it is unlikely that the hailstones under study were precisely at their terminal velocities but errors due to this should be small. If the observed hailstones had been seriously away from a stable mode of motion then measurable variations in their fallspeeds between successive image pairs should have been observed, whereas for these stones the RMS variation in vertical velocity was typically less than 0.1 ms^{-1}.

The equivalent data from the August 18 sample is plotted in Figure 8. On that day the pressure was 899 mb and the temperature was 22 C giving an air density of 1.06 kgm^{-3}. For both times under study the temperature and pressure readings were interpolated using the hourly reports from Penhold and Rocky Mountain House. Using these reports it was necessary to assume that pressure and temperature varied linearly in space and time. Though this is not a valid assumption it was unlikely to yield an erroneous value for the air density as a pressure change of 9 mb or a temperature change of 3 C (not together) would be required to alter the density value by 1%.

Figure 8 indicates that the curve (again C_D=0.6) is not

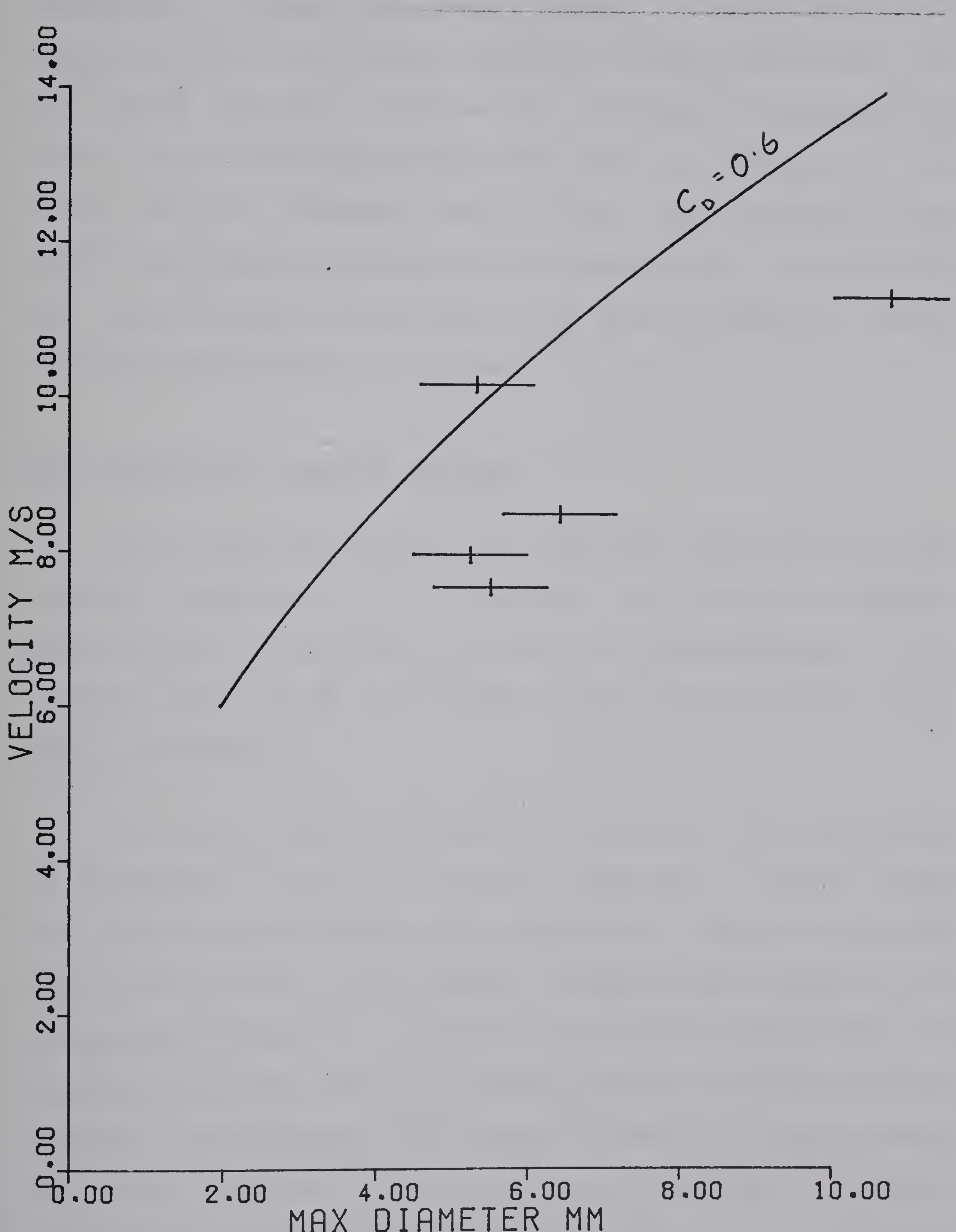

Figure 8. Vertical component of terminal velocity vs. maximum hailstone diameter for August 18 sample. The theoretical curve is given by equation 2.

a good fit for the data, and that a higher mean drag coefficient applies to these stones. Noting that it is related here to the maximum diameter, a drag coefficient of 0.9 would provide a better fit. This may be because the stones were a different shape from those of August 7; it could also be because fewer stones were tumbling. The latter possibility is discussed in section 4.5. It should be noted, however, that this is too small a sample to allow definite conclusions to be drawn.

4.5 Analysis of Vertical Motion.

In the previous section, an empirical relation for the vertical fallspeed of a hailstone was presented without consideration of the detailed motion of the hailstone. The evidence relating to the details of the vertical motion will now be discussed.

It is convenient to consider the motion of a hailstone in comparison to that of an oblate spheroid, a shape close to those commonly found among hailstones. Though more than half of the stones in the August 7 sample were conical it is at present difficult to consider these shapes separately, as no record has been found in the literature of studies of the detailed aerodynamics of conical bodies at appropriate Reynold's numbers, whereas useful studies of oblate spheroids are documented (List et al, 1973).

For non-spherical bodies, equation 2 becomes

$$V^2 = \frac{2\rho_i g}{\rho_a C_D} \times \frac{\text{Volume}}{\text{Area}} \tag{33}$$

where 'volume' is the volume of the body, 'area' is its cross-sectional area normal to its motion, and C_D is defined in terms of the cross-section normal to the flow. The orientation of the body is important as this determines both the 'area' and the drag coefficient (C_D) of the body. Most calculations of drag coefficient of freely falling bodies assume that the maximum area is presented to the flow. If drag coefficients based on this convention are used, then for an oblate spheroid, equation 33 becomes

$$V^2 = \frac{4}{3} \frac{\rho_i}{\rho_a} \frac{g}{C_D} D \tag{2}$$

where D is now the minor axis of the spheroid, since the ratio 'volume:area' has the value of Dx2/3. Roos and Carte (1973) suggest a drag coefficient of 0.50 to 0.55 for rough spheres, the precise value depending on the size of the roughness elements. Wind-tunnel studies at $Re=4\times10^4$ of an oblate spheroid of axis ratio 0.67 (List et al, 1973; Lozowski, personal communication) gave a drag coefficient, for the stable orientation (minor axis parallel to the undisturbed flow), of 0.602. These studies also show that if the oblate spheroid is tumbling about a major axis, and its cross-sectional area is assumed to be constant, the drag coefficient appropriate to its mean motion will be 0.348. For an oscillating spheroid the mean drag coefficient will

lie between these extreme values. The velocity curves (given by equation 2) corresponding to these extreme conditions (tumbling spheroid of axis ratio 0.67, sphere, and steady spheroid of axis ratio 0.67) are plotted in Figure 9 along with the data points for the August 7 sample, identified according to the axis ratio of the hailstones. For clarity the error bars have been omitted; their magnitude can be seen by comparison with Figure 7. The data for August 18 is similarly plotted in Figure 10. Hailstone fallspeeds are being compared to the fallspeeds of oblate spheroids. Equation 2 implies that the relevant dimension to consider is the minor axis so the hailstone dimension plotted is the minimum diameter.

If the quoted drag coefficients are representative of the hailstones under study then the distribution of data points with respect to the curves in Figure 9 indicates that the majority of these hailstones were not falling in a steady orientation. They were either tumbling or oscillating through large angles. It is unlikely that the latter situation could be maintained without tumbling setting in. The hypothesis that the hailstones are tumbling is further supported by observations from the data film. Successive images of stones are often at different orientations and continuous fall streaks vary in width, both indicating an oscillating or tumbling body. In the August 7 sample there were 18 stones that were identified as definitely tumbling or oscillating. These are plotted in

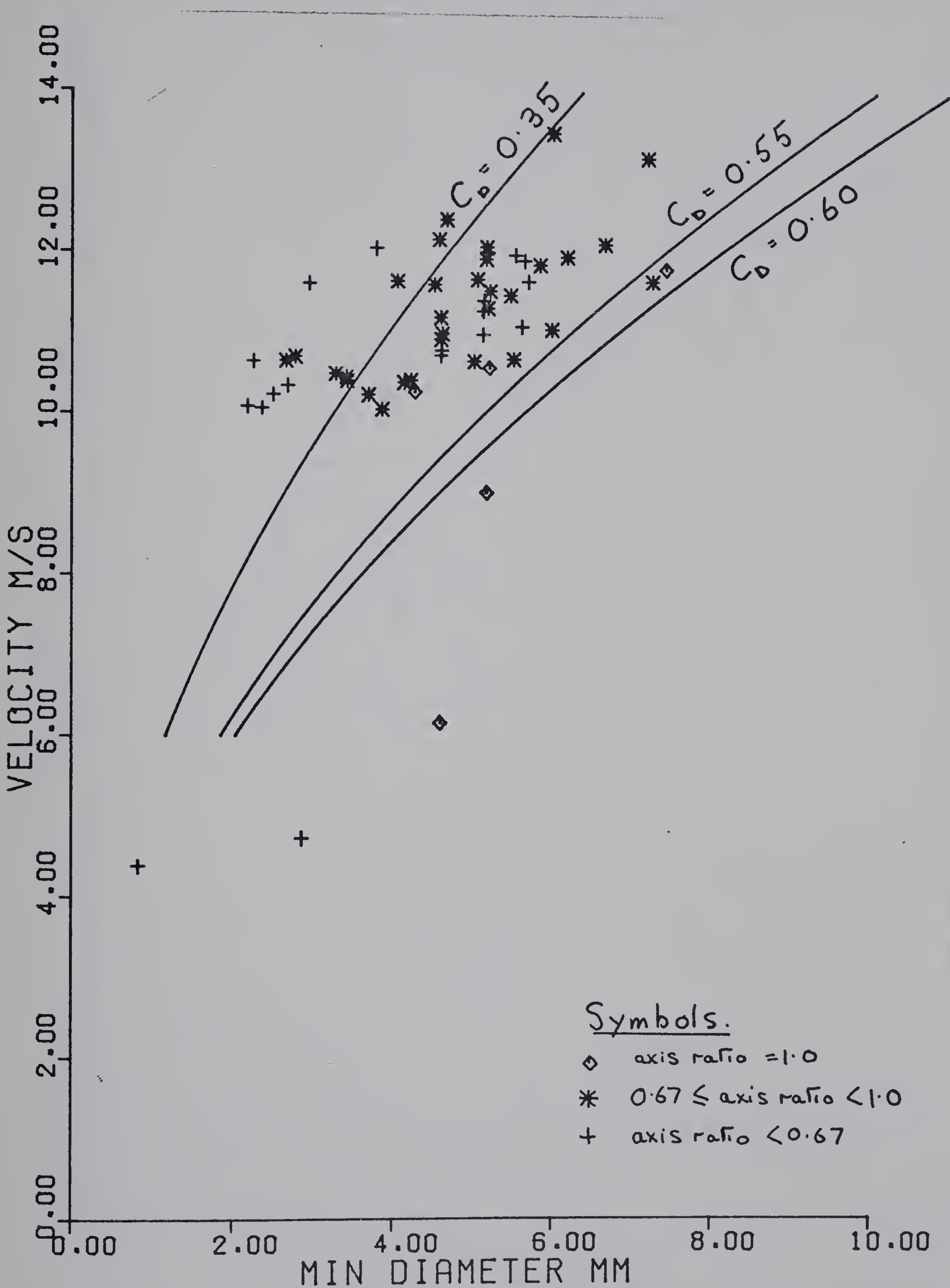

Figure 9. Vertical component of terminal velocity versus minimum hailstone diameter, for August 7 sample.

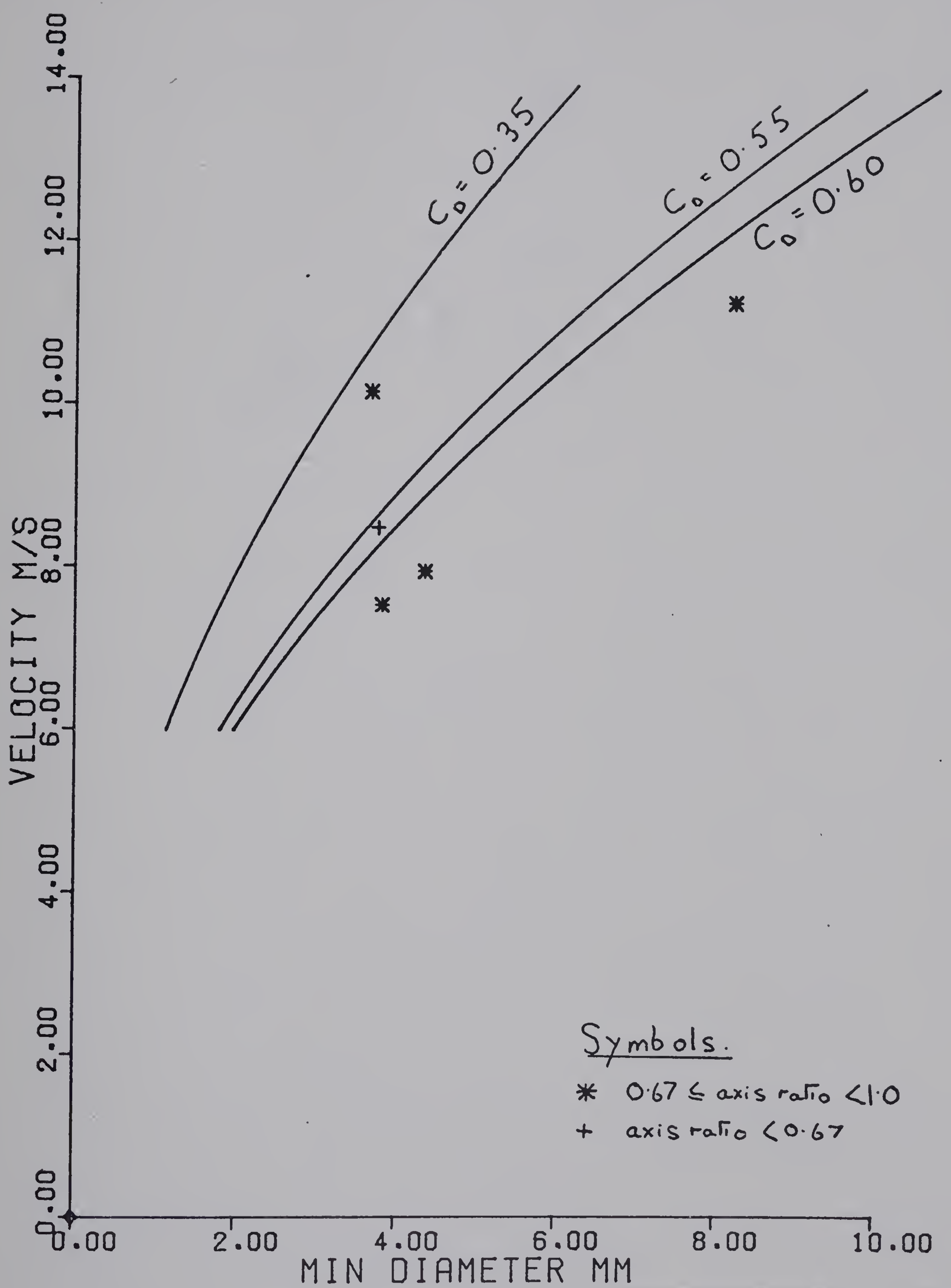

Figure 10. Vertical component of terminal velocity versus minimum hailstone diameter, for August 18 sample.

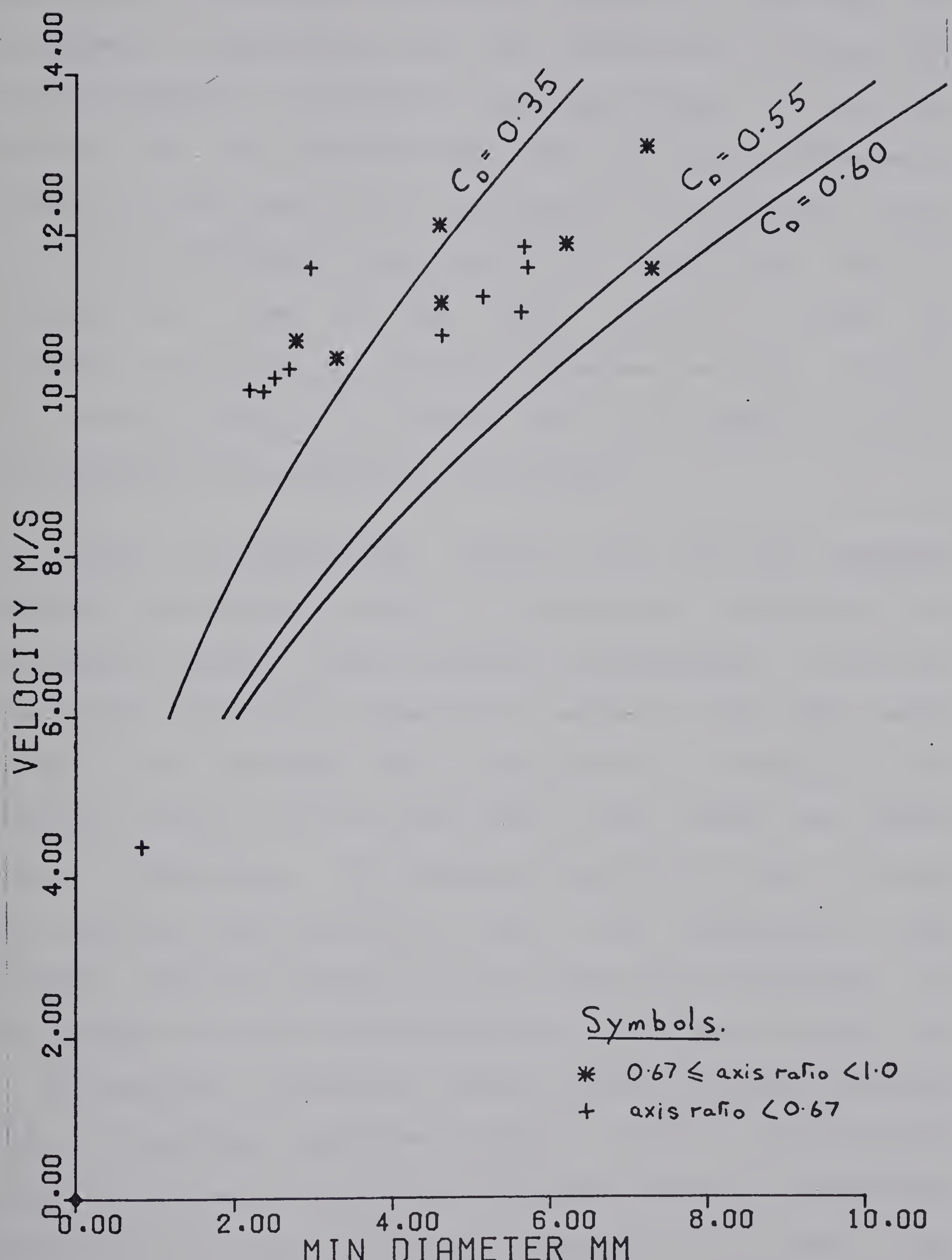

Figure 11. Vertical velocity component versus minimum hailstone diameter, for rotating stones in August 7 sample.

Figure 11 with the same curves as in Figure 9. This shows that most of the stones that were definitely tumbling had fallspeeds compatible with the theoretical values for tumbling bodies. For most of the other stones it was not possible to tell, by observing the film, whether they were tumbling or not, but if the hypothesis that hailstones with low drag coefficients are tumbling is correct then Figure 9 suggests that some of them were. Figure 10 seems to indicate that most of the stones observed on August 18 fell in a steady orientation, however this is too small a sample from which to draw definite conclusions.

Other possibilities giving rise to the observed velocity distribution must be considered. Variations in hailstone density would change the fallspeed. It may be that those few stones, observed on August 7, that fell much slower than expected were snow pellets or graupel of low density, though it is unlikely that these would not have melted completely. If stones are melting in fall and have wet surfaces this may reduce their drag coefficients and thereby cause the stones to fall faster than otherwise. It is possible that the fastest falling stones were falling in a streamlined orientation (minor axis horizontal) though this is generally considered to be an unstable orientation which could not be maintained for long periods. Systematic differences in the vertical variation of wind and temperature (and hence melting rate) might cause the differences in velocity distribution between the two samples

though it is likely that other factors such as hailstone shape are more important. It is probable that hailstone shape has a greater influence on fallspeed than has hitherto been realised and investigation of that requires a more extensive detailed study than has so far been possible.

Before any quantitative comment can be made regarding rotation rates, it is necessary that modifications be made to the experiment to improve the accuracy of the measurements and the resolution of the film images; these will be discussed in Chapter 5. It would also be helpful if studies were undertaken in a wind-tunnel to determine how drag coefficient varies with angle of attack for bodies other than oblate spheroids, in particular conical forms that are common in graupel and small hail.

Chapter 5. CONCLUSIONS.

5.1 Summary of Results.

The results of the main case study (August 7) show that a reasonable relation to determine the mean terminal velocity of a hailstone is given by

$$V = 13.9\ (D/\rho_a)^{1/2} \qquad (31),$$

where D is the hailstone's maximum diameter. For the majority of the stones studied this gave fall velocities to within 10%. However, looking at the results in detail, it was shown in Chapter 4 that many hailstones fell faster than the calculated terminal velocity of an oblate spheroid of axis ratio 0.67 with the same minimum dimension, falling with its minor axis vertical. This could have happened because the hailstones had lower drag coefficients, while maintaining the same orientation as the spheroid, but this is unlikely as the measurements of drag coefficients for spheroids were made on smooth models. Spheroids with different axis ratios have different drag coefficients, the drag coefficients for the stable orientation being higher than for spheres and those for rotating spheroids being generally less than for spheres. The difference in fallspeeds could arise if the hailstones were falling steadily with their minor axes horizontal, thus reducing their drag compared to the stable spheroid, but none were observed in this orientation and Roos and Carte (1973),

studying hailstone models, have observed that this is not a preferred orientation. The most likely explanation, which is supported by observations of 18 stones that were identified as tumbling, is that the hailstones were oscillating or tumbling in free-fall. This would decrease their drag, compared to that prevailing when their minor axes are vertical. It is thought that in many cases the hailstones were undergoing continuous rotation during free-fall, as oscillations through large angles would likely be required to produce the fallspeeds observed, angles of attack of 60° or greater being needed in order for an oblate spheroid's drag coefficient to be smaller than a sphere's. As commented in section 4.5, it is likely that hailstone shape has a great influence on fall velocity. More accurate predictive equations for fall velocity will need to include factors other than those already considered, such as shape and the effects of melting. The determination of these effects will require detailed and individual study of the fall of many more stones than have been included in any previous single study.

The rotation or oscillation rates cannot be determined precisely without farther experimental studies being undertaken. It may be possible to determine rotation rates by measuring the frequency of variations in fall-streak widths caused by tumbling stones but to do this accurately it would be desirable to sharpen the focussing of the cameras (discussed in section 5.3). It would also be useful

if a wind-tunnel investigation were carried out to determine the drag coefficients, at varying angles of attack, for conical bodies at Reynolds numbers appropriate to hail. This would allow the shape of a hailstone to be taken into account in attempting to explain its fall pattern, rather than comparing all experimental results to the theoretical results for oblate spheroids. Probably the most important contribution in this field is to be made by further direct observations of natural hail in free-fall using apparatus akin to that used in this study. Certain modifications are required in order to improve the quality and the quantity of the data collected, and these are discussed in this chapter.

5.2 Data to be Collected.

In order to reduce the errors in the measurement of hailstone dimensions and positions from photographs, it is desirable to increase the depth of field of the cameras, thereby reducing the circle of confusion for any image. A procedure for doing this is described in section 5.3. It is also desirable to be able to identify surface features of hailstones, so that a quantitative study of rotational motion may be made, and to increase the number of hailstones for which images appear on the films of both cameras. These last improvements are largely dependent on more controllable lighting.

There are a few additional measurements that it would

be useful to make at the time of each filming. In order to simplify the analysis, described in Chapter 3, the orientation of each camera should be measured, using a spirit level to determine the horizontal. Since air density must be determined in order to calculate the theoretical relations between velocity and hailstone dimension for comparison with measured fall velocities, it would be convenient if temperature and pressure were recorded at the time and location of filming. Measuring these parameters would be simpler and more accurate than interpolation from hourly reports at neighbouring stations.

5.3 Camera Focusing and Lighting.

In order to improve the sharpness of the film images, the cameras should be operated at a smaller aperture. An aperture of f/16, rather than f/3.5, would decrease the diameter of the circle of confusion for all images by a factor of 4.6, increasing the depth of field within which images can be considered to be well-focussed by a factor of approximately 7. The decrease in aperture will increase the effect of diffraction but this should not provide any problem as points separated on film by 10 μm should still be resolvable. The focussing improvement should help also to make hailstone surface features identifiable. As the decrease in the camera aperture will reduce the light incident on the film, it will be necessary to use faster film than the Tri-X (400 ASA) used in this study. If

sufficient contrast is obtainable it may not be necessary to use film that is 4.6 times faster, as implied by the decrease in aperture. A sufficient film speed may be achieved by using a film with a faster rating (e.g. Ilford HPS, 800 ASA) but probably sufficient speed may be obtained by forced processing of Tri-X. However this would produce a more grainy image than previously.

It is thought that surface features will be more easily identified if the only illumination of the photographic field is from the stroboscopes, and if continuous lighting is eliminated, since diffuse and continuous ambient light tends to eliminate the shadow necessary for the identification of texture. Very faint continuous lighting may be desirable in order to produce faint streaks connecting successive images of a single hailstone, but the majority of ambient light could be beneficially excluded. The balance between stroboscopic and continuous illumination required to give the most useful images on the chosen film will have to be determined experimentally before being used in a field programme. The blocking of ambient lighting could be accomplished by placing screens to the sides of the backdrop, which would then need to be higher. However it seems more practicable to perform the photography within a rigid darkened shaft (Sasyo, 1971), and a possible arrangement for this will be outlined in the next section.

5.4 Structural Modifications.

The analysis of the films would be simplified if the camera mountings were modified so as to prevent the possibility of a camera rotating slightly about the axis of its mounting bolt, and also if the mountings were fixed to a common base to prevent their moving independently of each other. This base should be mounted in a shock-free manner, such as sitting on a bed of foam rubber, to protect the cameras in transit.

If photography is to be carried out within a darkened shaft, as suggested above, it would be reasonable to mount this shaft within the van, thereby reducing the time taken to set up the photographic equipment once a site has been chosen. A 1 m^2 hole in the roof of the van (which could be covered when not in use) should admit sufficient hail to provide a significant sample. The total number of hailstones passing through the field of view would be decreased, but the improved conditions should increase the proportion that is successfully photographed. The walls of the shaft should extend several inches above the roof in order to reduce the number of stones bouncing off the roof and through the field of view. The top section of the shaft should be tapered, with its narrowest point at the top entrance, to minimise the number of hailstones ricocheting off the sides of the shaft. The lowest section should be tapered in the opposite sense to permit collection or

removal of the rain and hail falling through the shaft. The intermediate working section should have the cameras and stroboscopes mounted on a ledge set back from the shaft, in a similar construction to that used by Sasyo (1971). The shaft should still contain a plumb-line to identify the vertical.

Though it would simplify the analysis if the optic axes of the cameras were parallel (and for this they could be placed closer to each other than previously) or at right angles, I think it would be most beneficial to have both optic axes in a horizontal plane and separated by an appropriate angle to maximise the volume of space lying in the field of view of both cameras, within the shaft. If the optic axes were at right angles to each other the resultant dimensions of the apparatus would be inconveniently large for transportation. For example if the shaft to be viewed completely by both cameras had a cross-section of 1.5 m x 1.5 m, each camera would have to be placed 1.75 m away from the shaft and so the complete apparatus would be 3.25 m x 3.25 m. However if the cameras are seperated by 1.5 m and the optic axes are at 46.4° to each other, the same volume can be viewed while the overall dimensions of the equipment are only 1.5 m x 2.9 m. If a smaller sample volume is acceptable, the longer dimension may be reduced. A schematic representation of this shorter set-up is given in Figures 12 and 13. The linear dimensions are approximate and the angular data correspond to 28 mm lenses arranged so

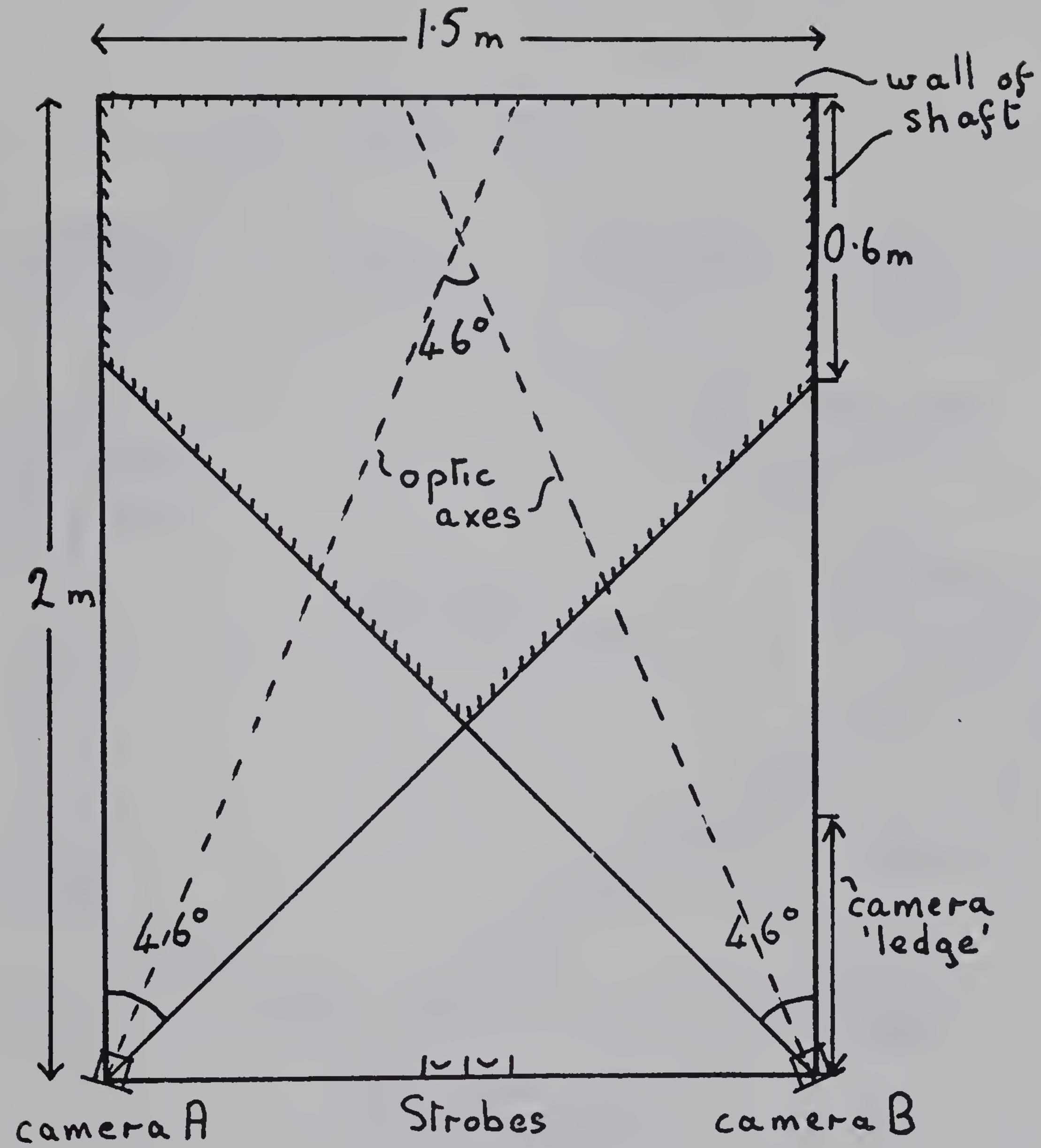

Figure 12. Plan view of a possible arrangement for cameras in an enclosed shaft. Hatched lines enclose the area in the field of view of both cameras.

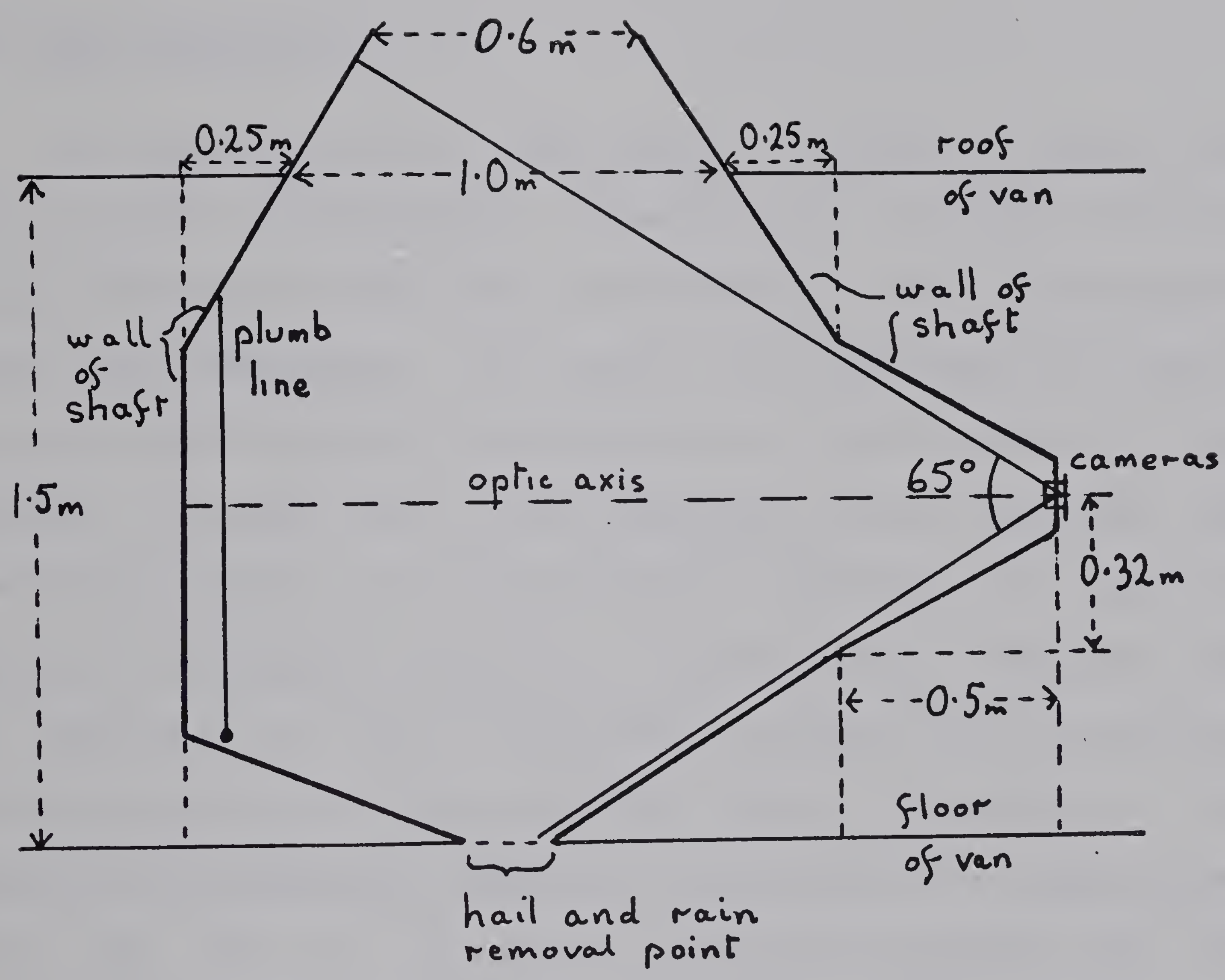

Figure 13. Vertical section of a possible arrangement for cameras in an enclosed shaft.

that the shorter side of each camera's film frame is horizontal. For the dimensions used, the area within the field of view of both cameras can be completely 'in focus' at f/16; that is, the diameter of the circle of confusion is everywhere smaller than 30 μm, which is the diameter regarded as acceptable by the lens manufacturer.

5.5 Data Analysis.

The methods used in this study to extract data from film proved satisfactory; however, if a study involving larger amounts of data were undertaken, some improvements would be desirable. It would be convenient to use a computerized digitizer to measure the coordinates of film images, though this would probably only automate the measuring process, an operator being required in order to identify successive images of a single stone. It would only be realistic to use a digitizer provided that it could be used in conjunction with projected film. Otherwise a vast amount of photographic printing would have to be undertaken. Once the data is stored in a computer-readable form, the analytic methods used in this study would be satisfactory for the calculation of spatial coordinates and dimensions of hailstones.

BIBLIOGRAPHY.

Atmospheric Environment Service of Canada, 1971: Manobs: Manual of standard procedures for surface weather observing and reporting. 6th edition. Environment Canada, Toronto. 307 pp.

Auer,A.H., 1972: Distribution of graupel and hail with size. Mon. Weather Rev. 100,325-328.

Bilham,E.G., and E.F.Relf, 1937: The dynamics of large hailstones. Quart. J. Roy. Meteor. Soc. 63, 149-162.

Cannon,T.W., 1974: A camera for photography of atmospheric particles from aircraft. Rev. Sci. Instrum. 45, 1448-1455.

Carte,A.E., 1971: Replication of hailstones. Weather 26, 289-291.

Douglas,R.H., 1964: Hail size distribution. Proc. 11th Radar Weather Conf. , Boston, AMS 146-149.

____, and W.Hitschfeld, 1959: Pattern of hailstorms in Alberta. Quart. J. Roy. Meteor. Soc. 85, 105-119.

Fichtl,G.H., 1971: The responses of rising or falling spherical wind sensors to atmospheric wind perturbations. J. Appl. Meteor. 10, 1275-1284.

Goldstein,H., 1950: Classical Mechanics. Addison-Wesley.

Goldstein,S., 1938: Modern Developments in Fluid Dynamics. Oxford Univ. Press.

Held,G., 1974: Ten years of hail observations in the Pretoria Witwatersrand area. J. De Recherches Atmosphériques 7, 185-197.

Knight,C.A., and N.C.Knight, 1970: The falling behaviour of hailstones. J. Atmos. Sci. 27, 672-681.

Kry,P.R., and R.List, 1974: Angular motions of freely falling spheroidal hailstone models. Phys. Fluids 17, 1093-1102.

List,R., 1959a: Zur Aerodynamik von Hagelkörnern. Z. Angew. Math. Phys. 10, 143-159.

____, 1959b: Der Hagelversuchskanal. Z. Angew. Math. Phys. 10, 381-415.

____, and R.S.Schemenauer, 1971: Free-fall behavior of planar snow crystals, conical graupel and small hail. J. Atmos. Sci. 28, 110-115.

____,U.W.Rentsch,A.C.Byram, and E.P.Lozowski, 1973: On the aerodynamics of spheroidal hailstone models. J. Atmos. Sci. 30, 653-661.

Lozowski,E.P.,M.M.Oleskiw, and T.M.Morrow, 1974: Hail Photography: An example of the use of high speed techniques under adverse conditions. Jour. Soc. Motion Picture and Television Engineers 84, 18-24.

Ludlam,F.H., 1950: The composition of coagulation elements in cumulonimbus. Quart. J. Roy. Meteor. Soc. 76, 52-58.

Mack,J.E., and M.J.Martin, 1939: The Photographic Process. McGraw-Hill. 586pp, Chap. 3.

Macklin,W.C., and F.H.Ludlam, 1961: The fallspeeds of hailstones. Quart. J. Roy. Meteor. Soc. 87, 72-81.

____,L.Merlivat, and C.M.Stevenson, 1970: The analysis of a hailstone. Quart. J. Roy. Meteor. Soc. 96, 472-486.

Mason,B.J., 1971: The Physics of Clouds, 2nd edition. Clarendon Press. 671pp.

Miller,M.J., and R.P.Pearce, 1974: A three-dimensional primitive equation model of cumulonimbus convection. Quart. J. Roy. Meteor. Soc. 100, 133-154.

Mossop,S.C., 1971: Some hailstones of unusual shape. Weather 26, 222.

Paul,A.H., 1973: The heavy hail of 23-24 July 1971 on the Western Prairies of Canada. Weather 28, 463-471.

Quick,G.R., 1974: Acceleration analysis of crop cutting by high-speed photography. 116th International Technical Conf., Soc. Motion Picture and Television Engineers , Toronto, Nov. 1974.

Roos,D.v.d.S., 1972: A giant hailstone from Kansas in free fall. J. Appl. Meteor. 11, 1008-1011.

____, and A.E.Carte, 1973: The falling behaviour of oblate and spiky hailstones. J.de Rech. Atmos. 7, 39-52.

Sasyo,Y., 1971: Study of the formation of precipitation by the aggregation of snow particles and the accretion of cloud droplets on snowflakes. Papers in Meteorology and Geophysics. Met. Res. Inst., Tokyo 22, 69-142.

Schumann,T.E.W., 1938: The theory of hailstone formation. Quart. J. Roy. Meteor. Soc. 64, 3-21.

Shands,A.L., 1944: The hail-thunderstorm ratio. Monthly Weather Rev. 72, 71.

Smith,A.M.O., 1953: On the motion of a tumbling body. J. Aero. Sci. 20, 73-84.

Smith,E.H., 1971: Autorotating wings: an experimental investigation. J. Fluid Mech. 50, 513-534.

Stringham,G.E.,D.B.Simons, and H.P.Guy, 1969: The behavior of large particles falling in quiescent liquids: Sediment transport in alluvial channels. U.S. Govt. Printing Off.

Strong,G.S., 1974: The objective measurement of Alberta hailfall. M.Sc. Thesis, Meteorology Division, Dept. of Geography, University of Alberta. 182pp.

Suzuki,T., 1973: An Introduction to the Canon F-1. Public Relations and Advertising Div., Canon Inc., Tokyo, Japan.

Warner,C., 1973: Radar and photo studies of Alberta hailstorms. Weather 28, 293-299.

Wegener,A., 1911: Thermodynamik der Atmosphäre. Leipzig.

Williamson,R.E., and P.B.MacCready, 1968: Aircraft probing of hailstorms, Final Report, Contract no. 5-2-67, Meteorology Research Inc., Altadena, Calif., 37 pp.

Willmarth,W.W., and R.L.Enlow, 1969: Aerodynamic lift and moment fluctuations of a sphere. J. Fluid Mech. 36, 417-432.

____,N.E.Hawk, and R.L.Harvey, 1964: Steady and unsteady motions and wakes of freely falling disks. Phys. Fluids 7, 197-208.

Wojtiw,L., and P.W.Summers, 1972: The economic impact and regional variation of hail damage in Alberta. Alberta Hail Studies 1972, Research Council of Alberta, Edmonton. Hail Studies Report 72-2 , 6-11.